Published in final edited form as:
Cancer Discov. 2021 May 01; 11(5): 1228–1247. doi:10.1158/2159-8290.CD-20-0652.

MNK inhibition sensitizes *KRAS*-mutant colorectal cancer to mTORC1 inhibition by reducing eIF4E phosphorylation and c-MYC expression

John R. P. Knight[1], **Constantinos Alexandrou**[1], **George L. Skalka**[1,2], **Nikola Vlahov**[1], **Kathryn Pennel**[3], **Leah Officer**[2], **Ana Teodosio**[2], **Georgios Kanellos**[1], **David M. Gay**[1,3,16], **Sebastian May-Wilson**[1,17], **Ewan M. Smith**[1], **Arafath K. Najumudeen**[1], **Kathryn Gilroy**[1], **Rachel A. Ridgway**[1], **Dustin J. Flanagan**[1], **Rachael C. L. Smith**[1,3], **Laura McDonald**[4], **Craig MacKay**[4], **Anne Cheasty**[5], **Kerri McArthur**[5], **Emma Stanway**[5], **Joshua D. Leach**[1,3], **Rene Jackstadt**[1], **Joseph A. Waldron**[1], **Andrew D. Campbell**[1], **Georgios Vlachogiannis**[6], **Nicola Valeri**[6,7], **Kevin M. Haigis**[8,9,10], **Nahum Sonenberg**[11], **Christopher G. Proud**[12,13], **Neil P. Jones**[5], **Martin E. Swarbrick**[5], **Heather J. McKinnon**[4], **William J. Faller**[1,18], **John Le Quesne**[2,3,14,15], **Joanne Edwards**[3], **Anne E. Willis**[2], **Martin Bushell**[1,3], **Owen J. Sansom**[1,3,*]

[1]CRUK Beatson Institute, Garscube Estate, Switchback Road, Glasgow, G61 1BD. UK

[2]MRC Toxicology Unit, University of Cambridge. Tennis Court Rd, Cambridge CB2 1QW. UK

[3]Institute of Cancer Sciences, University of Glasgow. G61 1QH. UK

[4]Drug Discovery Unit, CRUK Beatson Institute, Glasgow, G61 1BD, UK

[5]CRUK Therapeutic Discovery Laboratories, Jonas Webb Building, Babraham Research Campus, Cambridge CB22 3AT, UK

[6]Division of Molecular Pathology, The Institute of Cancer Research, London, SM2 5NG, UK

[7]Department of Medicine, The Royal Marsden NHS Foundation Trust, London, SM2 5PT, UK

[8]Department of Cancer Biology, Dana-Farber Cancer Institute, Boston, MA 02215, USA

[9]Department of Medicine, Brigham & Women's Hospital and Harvard Medical School, Boston, MA 02115, USA

[*]Correspondence: Prof. Owen J. Sansom. 01413307125. o.sansom@beatson.gla.ac.uk.
[16]Present address: Biotech Research and Innovation Centre, Københavns Universitet 2200, Denmark.
[17]Present address: Old Medical School, The University of Edinburgh, Edinburgh EH8 9AG, UK
[18]Present address: NKI, Plesmanlaan 121, 1066 CX Amsterdam, Netherlands.

Author contributions

Conceptualization: JRPK, WJF, AEW, MB, OJS. Methodology: JRPK, RAR, JDL, RJ, WJF, OJS. Investigation: JRPK, CA, GS, N. Vlahov, KP, LO, AT, GK, DG, SMW, EMS, AKN, KG, RAR, DJF, RCLS, LM, AC, KM, ES, JAW, ADC, WJF. Writing – Original Draft: JRPK, MB, OJS. Writing – Review and Editing: JRPK, JE, AEW, MB, OJS. Funding Acquisition: NPJ, MES, HJM, JE, JLQ, AEW, MB, OJS. Resources: GV, N. Valeri, KMH, NS, CGP. Supervision: JRPK, CM, NPJ, MES, HJM, WJF, JLQ, JE, AEW, MB, OJS.

Conflict of interest statement

CA, GK, CM, AC, ES, NPJ, MES, HJM, MB and OJS were funded by Cancer Research Technology Limited (a wholly owned subsidiary of Cancer Research UK) during the conduct of the study. OJS received funding from Novartis and Astra Zeneca outside the submitted work. CGP reports a patent pending for MNK inhibitors. NS has served on the SAB and is a minor stockholder of Effector Pharmaceuticals. N. Valeri reports personal fees from Bayer, Eli Lilly and Pfizer, and funding from Menarini BioSystems, all outside the submitted work. All other authors declare no potential conflicts of interest.

Europe PMC Funders Author Manuscripts

[10]Department of Cell Biology, Harvard Medical School, Boston, MA 02115, USA

[11]Department of Biochemistry and Goodman Cancer Research Center, McGill University, Montreal, QC H3A 1A3, Canada

[12]Lifelong Health, South Australian Health and Medical Research Institute, North Terrace, Adelaide, SA 5000, Australia

[13]Department of Biological Sciences, University of Adelaide, Adelaide, SA 5005, Australia

[14]Leicester Cancer Research Centre, University of Leicester, Leicester, LE2 7LX, UK

[15]Glenfield Hospital, Leicester University Hospitals NHS Trust, Leicester, LE3 9QP, UK

Abstract

KRAS-mutant colorectal cancers (CRC) are resistant to therapeutics, presenting a significant problem for ~40% of cases. Rapalogs, which inhibit mTORC1 and thus protein synthesis, are significantly less potent in *KRAS*-mutant CRC. Using *Kras*-mutant mouse models and mouse- and patient-derived organoids we demonstrate that KRAS with G12D mutation fundamentally rewires translation to increase both bulk and mRNA-specific translation initiation. This occurs via the MNK/eIF4E pathway culminating in sustained expression of c-MYC. By genetic and small molecule targeting of this pathway, we acutely sensitize $KRAS^{G12D}$ models to rapamycin via suppression of c-MYC. We show that 45% of CRCs have high signaling through mTORC1 and the MNKs, with this signature correlating with a 3.5-year shorter cancer-specific survival in a subset of patients. This work provides a c-MYC-dependent co-targeting strategy with remarkable potency in multiple *Kras*-mutant mouse models and metastatic human organoids and identifies a patient population who may benefit from its clinical application.

Keywords

colorectal cancer; mouse models; protein synthesis; translation; *KRAS*; eIF4E; MNK; mTORC1; c-MYC

Introduction

Genomic sequencing has comprehensively characterized the mutational landscape of colorectal cancer (CRC)(1,2) finding activating mutations in the *KRAS* proto-oncogene in >40% of patients. Oncogenic mutations in *KRAS* result in the constitutive activation of proliferative signaling cascades, fueling tumor progression, and conferring resistance to standard-of-care first-line therapies. Therapies targeting KRAS or its downstream effector pathways have failed to materialize in the clinic (3), although a compound specifically targeting mutant $KRAS^{G12C}$ has recently show efficacy in multiple solid tumors (4). Given the association of KRAS-pathway aberrations with therapy resistance and disease recurrence in CRC, and a similarly dismal outlook for *KRAS*-mutant patients with other indications, new treatment strategies are urgently needed.

Inactivation of the APC tumor suppressor, which leads to deregulation of pro-proliferative WNT signaling, is a key initiating event in intestinal adenoma formation. We previously

showed that *Apc*-deficient enterocytes are dependent on mTORC1 to promote translation elongation, sensitizing *Apc*-deficient adenomas to the mTORC1-inhibitor rapamycin (5). This has been recapitulated clinically with rapamycin regressing colonic polyps in familial adenomatous polyposis (FAP) patients predisposed to adenoma formation due to germline *APC* mutation (6). Despite this success in *APC*-deficient adenomas, sporadic CRC patients fail to benefit from rapalogs (rapamycin and its analogues) with those harboring oncogenic *KRAS* mutations performing even worse (7–9). Importantly, mice bearing *Apc*-deficient colonic tumors exhibited significant regression with rapamycin, while counterparts with *Apc* loss and KRAS activation failed to respond (10). These considerations underscore the need to identify therapeutic vulnerabilities of *KRAS*-mutant tumors that may synergize with rapalogs.

Colorectal cancer has been classified into 4 consensus molecular subtypes (CMSs)(1). CMS1 is highly immune infiltrated, with mismatch repair mutations common. CMS4 is highly stromal and has the worst prognosis. CMS2 and 3 are characterized by low infiltration and are primarily comprised of epithelial tumor cells. CMS2 has high WNT and MYC signatures and CMS3 is enriched for *KRAS* mutation and exhibits metabolic alterations. The Glasgow Microenvironment Score (GMS) segregates CRCs by immune and stromal infiltration (11), with GMS0 being immune infiltrated (roughly correlating with CMS1), GMS2 being highly stromal with the worst prognosis (akin to CMS4) and GMS1 being the least infiltrated (in line with CMS2/3). The immunologically pauce tumors in CMS2/3 and GMS1 are unresponsive to checkpoint inhibition and thus require new therapeutics targeting key cancer-cell-intrinsic pathways.

In cancer, deregulation of mRNA translation underpins the increased bulk protein synthesis that sustains the elevated rates of cell proliferation, alongside upregulation of oncogene expression through preferential mRNA recruitment to the ribosome (12). Phosphorylation of the translation initiation factor eIF4E on serine 209 (S209) is downstream of many oncogenic pathways; KRAS can signal to eIF4E via MAPK or p38 signaling (13–16). Both of these pathways converge on the MAP kinase-interacting serine/threonine-protein kinases MNK1 and MNK2, which in turn are the only kinases that phosphorylate eIF4E at S209 (17,18). MNK-mediated eIF4E phosphorylation has been implicated in solid and liquid cancers (19–25).

Deletion of the *Mnks* is developmentally tolerated and has no adverse effects in adult mice (17) as is the expression of a non-phosphorylatable S209A point mutant of eIF4E (19). The tolerability and efficacy of genetic deletion of the MNKs in numerous models have prompted the development of MNK inhibitors. Foremost among these is eFT508, a potent inhibitor with excellent oral bioavailability and pharmacokinetics, that has progressed into phase II clinical trials (24,26). Mechanistically, phospho-eIF4E (P-eIF4E) drives an oncogenic translation program, via a set of ‘P-eIF4E dependent’ transcripts, including *C-myc*, *Cyclin D1*, *Cyclin E* and *Mcl1* (22,23). How P-eIF4E specifically promotes translation of oncogenic mRNAs remains unclear. In fact, phosphorylation of serine 209 is not required for translation to proceed and reduces the affinity of eIF4E for mRNA (27,28). To date, the increased translation of these proliferative transcripts has only been correlated with P-eIF4E. There remains a paucity of data directly demonstrating the importance of these ‘P-eIF4E-

dependent' mRNAs on the tumor phenotype. This lack of understanding limits therapeutic exploitation of this pathway.

Here, we analyze the role of oncogenic *Kras* mutation on protein synthesis and tumorigenesis in the intestine. Using genetically engineered mouse models (GEMMs) we demonstrate that KRAS activation enhances protein synthesis and drives proliferation. We identify upregulated translation initiation downstream of KRAS which coincides with increased MNK/eIF4E signaling. KRAS overrides signaling to translation from mTORC1, rendering proliferation resistant to rapamycin and altering the molecular mode of rapamycin *in vivo*. Genetic or pharmacological disruption of the MNK/eIF4E axis alone is insufficient to suppress tumorigenesis. However, co-targeting the pathway with inhibition of mTORC1 using rapamycin shows a significant benefit in multiple mouse and human organoid models. We observe that this involves the suppression of total protein synthesis by rapamycin and the regulation of c-MYC expression by P-eIF4E. We also show that biomarkers for these pathways co-occur in CRC patients and correlate with poor survival in patients with GMS1 tumors, accounting for 1 in 5 patients in total. Together, our work defines a role for oncogenic KRAS in driving protein synthesis and uncovers a druggable vulnerability downstream of KRAS with multi-cancer therapeutic potential.

Results

Mutant *Kras* confers resistance to rapamycin

Given that *KRAS* mutations correlate with resistance to rapamycin, we first examined the impact of rapamycin following oncogenic mutation of *Kras*. This was achieved through the generation of $VillinCre^{ER}\ Apc^{fl/fl}\ Kras^{G12D/+}$ mice (referred to as APC KRAS short-terms), whose responses were compared to $VillinCre^{ER}\ Apc^{fl/fl}$ mice (referred to as APC short-terms) expressing wild-type *Kras*. Upon induction with intraperitoneal injection of tamoxifen these mice exhibit intestinal hyper-proliferation. Hyper-proliferation in $VillinCre^{ER}\ Apc^{fl/fl}$ intestines is reduced by rapamycin treatment due to suppression of hyperactive mTORC1 signaling (Figure 1A), consistent with our previous publication (5). In comparison, rapamycin treatment of $VillinCre^{ER}\ Apc^{fl/fl}\ Kras^{G12D/+}$ mice had only a modest effect on proliferation (Figure 1A).

In parallel, we generated $VillinCre^{ER}\ Apc^{fl/+}\ Kras^{G12D/+}$ mice (i.e. now heterozygous for the *Apc* flox allele – referred to as APC KRAS tumor model mice) that develop intestinal adenomas upon loss of the second copy of *Apc*. These were aged until displaying signs of intestinal disease and compared with a cohort of $VillinCre^{ER}\ Apc^{fl/+}$ mice (APC tumor model mice). The expression of oncogenic KRAS reduced the latency of our tumor model, from 227 to just 63days (Figure S1A), consistent with previous reports (29,30). Mice expressing oncogenic KRAS exhibit more colonic adenomas, with a smaller increase in adenomas of the small intestine (Figure S1B). Using this model, we tested the effect of rapamycin on tumor initiation and progression by treating APC KRAS tumor model mice with rapamycin or vehicle from 5days post induction, seeing no difference in survival (Figure 1B). We have previously demonstrated complete suppression of an APC ageing model by rapamycin treatment (5). Together these findings indicate that rapamycin does not inhibit the formation or growth of adenomas in the presence of oncogenic $Kras^{G12D}$

mutation. Recent literature suggests that specific KRAS mutations have different potencies for transformation, dependent on engaging downstream effector pathways. In colorectal cancer $KRAS^{A146T}$ can drive anti-EGFR resistance, but correlates with better survival than $KRAS^{G12D}$, and is less potent in cooperating with *Apc* loss in mouse models (31). In contrast to anti-EGFR resistance, we find that expression of $KRAS^{A146T}$ is insufficient to give intrinsic resistance to rapamycin *in vivo* (Figure S1C).

Next, we utilized another tumor model, the $Apc^{1322T/+}$ mutant mouse, which develops intestinal adenomas, akin to FAP patients. Treatment of symptomatic $Apc^{1322T/+}$ mice, wild-type for *Kras*, with rapamycin for 10days resulted in a reduction in proliferation in established adenomas (Figure 1C). Engineering these mice to express oncogenic $KRAS^{G12D}$ for the final 3days of rapamycin treatment completely reversed the suppression of proliferation (Figures 1C and S1D), showing that acute $KRAS^{G12D}$ activation is sufficient to provide rapid and complete resistance to rapamycin.

Mutant *Kras* promotes translation initiation and alters the molecular effects of rapamycin

We next analyzed *ex vivo* organoids generated from the small intestines of APC or APC KRAS short-term mice. These organoids recapitulated the *in vivo* phenotype with APC organoids giving a reduced metabolic readout used as a surrogate for proliferation following rapamycin treatment, whereas APC KRAS organoids were unaffected (Figures 2A and S2A). APC organoids treated with rapamycin demonstrate a marked reduction in protein synthesis measured by ^{35}S methionine incorporation (Figure 2B). APC KRAS organoids also demonstrate 25% reduction in protein synthesis (Figure 2A and B).

To gain a mechanistic insight into the action of rapamycin, we analyzed the rates of translation initiation and elongation using sucrose density ultra-centrifugation and harringtonine run-off analyses. The APC KRAS model exhibits more polysomes but does not differ in translation elongation rate, compared to the APC model (Figures S2B and S2C), indicative of increased translation initiation driven by $KRAS^{G12D}$. Following rapamycin treatment, *Apc*-deficient cells respond by slowing elongation and retaining more ribosomes within polysomes (Figures S2B and S2C). In contrast, in response to rapamycin APC KRAS cells load fewer ribosomes into their polysomes with no change in elongation rate, indicating impaired initiation. This demonstrates an altered mode of action of rapamycin – from an inhibitor of elongation in *Apc*-deficient cells to an inhibitor of initiation following mutation of *Kras*.

Translation elongation is slowed following rapamycin treatment in the APC model due to increased P-eEF2 (5). Consistent with no effect on translation elongation in APC KRAS intestines, rapamycin treatment did not impact P-eEF2 in this genotype (Figures S2D and S2E). Rapamycin remains an effective inhibitor of S6K signaling downstream of mTORC1, with phosphorylation of its substrate P-RPS6 S240/4 slightly suppressed in the APC KRAS model, while P-4E-BP1 T37/46 was significantly decreased by rapamycin. Therefore, KRAS-activation supersedes the regulation of P-eEF2 by mTORC1, such that inhibition of mTORC1 no longer affects P-eEF2 levels. mTORC1/S6K can also signal to the initiation factors eIF4B and eIF4G (32–34). We find these initiation factors responsive to rapamycin in both APC and APC KRAS organoids, demonstrating a functional link between mTORC1

and initiation, which, as well as decreased P-4E-BP1, may explain how rapamycin suppresses translation in the APC KRAS model (Figures S2B, S2D and S2E).

From this we conclude that KRAS activation with *Apc* deletion upregulates protein synthesis by promoting translation initiation. We also observe a functional uncoupling of protein synthesis from proliferation, with rapamycin treatment of APC KRAS organoids resulting in suppressed protein synthesis without impacting proliferation. We, therefore, reasoned that to successfully target translation in this model we need to either suppress translation further or selectively suppress translation of pro-proliferative messages. To investigate, we focused on translation initiation given its importance following KRAS activation.

P-eIF4E is enhanced by $Kras^{G12D}$ mutation

Phosphorylation of eIF4E is known to occur downstream of KRAS signaling (35). We observed increased P-eIF4E in APC KRAS short-term intestines and within colonic adenomas from the APC KRAS tumor model compared with APC counterparts (Figures 3A and S3A). Consistently, western blot analysis showed a stepwise increase in P-eIF4E to APC and then APC KRAS cultures compared with wild-type organoids (Figure S3B). Interestingly, P-eIF4E was lower in intestines expressing $Kras^{A146T/+}$ (Figure S3C), consistent with the response to rapamycin treatment seen in tumors with this *Kras* allele (Figure S1C). Oncogenic BRAF is also capable of signaling through the same pathways to P-eIF4E. P-eIF4E was variable in $Braf^{V600E/+}$ mouse intestines (Figure S3C), suggesting there may be role for this pathway in the ~10% of patients with these mutations.

We next sought to attenuate P-eIF4E and observe its effect on tumorigenesis in $Kras^{G12D}$ driven models. Genetic alteration of eIF4E serine 209 to alanine prevents upstream signaling from the MNKs and is tolerated *in vivo* (19). We therefore generated $VillinCre^{ER}$ $Apc^{fl/(fl\ or\ +)}$ $Kras^{G12D/+}$ $Eif4e^{S209A/S209A}$ mice, which have a homozygous knock-in of eIF4E S209A (APC KRAS eIF4E KI short-term or tumor models). The onset of intestinal neoplasia was not significantly different in the APC KRAS eIF4E KI tumor model compared to APC KRAS controls, and mice developed a similar tumor burden (Figure S3D).

Given that rapamycin suppresses protein synthesis via translation initiation in the APC KRAS model, we reasoned that combining rapamycin with targeting of P-eIF4E may be beneficial. Rapamycin treatment of APC KRAS eIF4E KI mice from an early time-point (5days) resulted in a 65% extension of survival compared with rapamycin-treated APC KRAS mice (Figure S3E). APC KRAS eIF4E KI mice were then treated with rapamycin at a late timepoint, when bearing intestinal adenomas. These animals exhibited a significant reduction in adenoma proliferation after 5days of treatment (Figure 3B), and a four-fold extension of survival (Figure S3F and G). APC KRAS mice (wild-type for *Eif4e*) treated with rapamycin at the same stage of intestinal disease gained no benefit from rapamycin (Figure 3B). Consistent with this, we observed a reduction in intestinal proliferation in the APC KRAS eIF4E KI short-term model following rapamycin treatment (Figure 3C), and in *ex vivo* organoids from these mice when treated with rapamycin (Figure S3H). P-eIF4E was absent in mice bearing the S209A mutation (Figure 3C). Rapamycin did not affect P-eIF4E in the *Eif4e* wild-type APC KRAS short-term model (Figure S3A and S3I), thereby

excluding this potential mechanism for disruption of P-eIF4E enhancing rapamycin sensitivity.

P-RPS6 S240/4 and P-eIF4E S209 co-occur in colorectal cancer patients

The efficacy of targeting P-eIF4E in combination with mTORC1 inhibition indicates the importance of these pathways in CRC. To address the clinical importance of these pathways we stained a tissue microarray (TMA) containing tumors from 192 patients for P-eIF4E S209 and P-RPS6 S240/4, the latter as a readout of mTORC1 activity (Figure 3D). Almost 50% (80/170) of patients had high levels of both P-eIF4E and P-RPS6, contributing to a significant positive correlation between the two (Figure 3E). Thus, high MNK and mTORC1 activities co-occur in a significant fraction of CRC patients, identifying a population of patients who may benefit from co-targeting.

Mnk1/2 deletion combines with rapamycin to suppress KRAS-driven proliferation

The increase in P-eIF4E indicates heightened signaling through the MNKs. We therefore generated *VillinCre*^{ER} *Apc*$^{fl/(fl\ or\ +)}$ *Kras*$^{G12D/+}$ *Mnk1*$^{-/-}$ *Mnk2*$^{-/-}$ mice (referred to as APC KRAS MNK1/2 KO short-term or tumor models), that are germline knockout for both *Mnk1* and *Mnk2* (17), to assess the importance of these kinases. In parallel, we generated VillinCre^{ER} *Apc*$^{fl/(fl\ or\ +)}$ Kras$^{G12D/+}$ with single knockout of the either *Mnk1* or *Mnk2*. Deletion of *Mnk2* had a greater effect on P-eIF4E than deletion of *Mnk1* (Figure 4A), consistent with higher expression of *Mnk2* in the mouse intestine (Figure S4A). *Mnk1* and *Mnk2* are expressed throughout the intestinal epithelium of APC and APC KRAS mice (Figure 4B). *Mnk2* expression appears to be increased in APC KRAS compared with APC intestines, as confirmed by qPCR for each *Mnk* transcript (Figure 4C). BaseScope also confirmed the lack of *Mnk1* and *Mnk2* transcripts in APC KRAS mice with *Mnk* knockouts (Figure S4B). Deletion of both *Mnk1* and *Mnk2* abolished P-eIF4E *in vivo* (Figure 4A), as it did in organoids (Figure S4C). While APC KRAS organoids harboring *Mnk1* or *Mnk2* knockouts displayed reduced P-eIF4E levels relative to their WT counterparts, *Mnk1* deletion had a greater effect on P-eIF4E in organoid cultures than in *in vivo* experiments. The reasons for this are unclear but may relate to a greater role of the kinase in culture, or a lack of compensation by MNK2.

Single or double deletion of the *Mnks* in the APC KRAS tumor model had no effect on survival compared to mice expressing both *Mnks* (Figure S4D). APC KRAS MNK1/2 KO mice, administered rapamycin when showing late-stage symptoms of intestinal disease, survived 10 times longer than either vehicle treated APC KRAS MNK1/2 KO mice or rapamycin-treated APC KRAS mice (Figure 4D). Similarly, in the short-term model, APC KRAS MNK1/2 KOs showed partial suppression of proliferation compared to APC KRAS controls and when combined with rapamycin, exhibited reduced hyper-proliferation (Figure 4E). We observed a stepwise reduction in the effect of combination with rapamycin in APC KRAS models with *Mnk1* knockout followed by *Mnk2* knockout and finally to *Mnk1* and *Mnk2* knockouts in both the tumor and short-term models (Figure S4E, S4F, S4G and S4H). This dose-dependent nature of *Mnk* knockout is encouraging for drug targeting, suggesting a wide therapeutic window.

Europe PMC Funders Author Manuscripts

Next, we employed an orthotopic approach whereby *VillinCre^{ER} Apc$^{fl/fl}$ Kras$^{G12D/+}$* or *VillinCre^{ER} Apc$^{fl/fl}$ Kras$^{G12D/+}$ Mnk1$^{-/-}$ Mnk2$^{-/-}$* mice received a local injection of tamoxifen into the submucosa of the distal colon, producing a single colonic polyp which can be longitudinally monitored by colonoscopy (36,37). APC KRAS MNK1/2 KO mice treated with rapamycin, survived significantly longer than untreated APC KRAS or APC KRAS MNK1/2 KO mice (Figures 4F and S4I). Two out of four APC KRAS MNK1/2 KO mice survived to 200days post-induction, compared with a mean survival of only 29days in APC KRAS controls. Thus, genetically targeting the MNK/eIF4E pathway in combination with rapamycin treatment suppresses tumorigenesis. We next explored the mechanism behind this successful treatment.

P-eIF4E and mTORC1 cooperate to regulate c-MYC expression

Sucrose density gradients of extracts from APC KRAS eIF4E KI and APC KRAS MNK1/2 KO short-term model mice show that rapamycin slightly decreased polysome abundance in both cases (Figures S5A and S5B), similar to APC KRAS mice, indicating that rapamycin remains an inhibitor of translation initiation. The rate of ribosome run-off was unchanged by rapamycin treatment of either APC KRAS eIF4E KI or APC KRAS MNK1/2 KO organoids (Figures S5C and S5D). Therefore, the sensitization to rapamycin in these two genotypes is not due to an alteration in its mode of action to a translation elongation inhibitor seen in the APC models. Rapamycin is an effective inhibitor of protein synthesis in all genotypes analyzed (Figure S5E), and the genetic targeting of *Mnk* or *Eif4E* did not alter the effect of rapamycin on phosphorylation of eEF2 or RPS6 S240/4 (Figure S5F).

Protein synthesis rates were comparable between rapamycin-treated APC KRAS organoids that are not suppressed and rapamycin-treated APC KRAS eIF4E KI or APC KRAS MNK1/2 KO organoids where cell metabolic capacity was attenuated (Figure S5E). Interestingly, this data also indicates that, in the absence of rapamycin, *Mnk* deletion reduces protein synthesis. MNK suppression rarely has a great effect on global protein synthesis, although similar data to that presented here have been shown in two separate reports using prostate cancer cells (38,39). Therefore, the suppression of bulk protein synthesis is not the mechanism behind the efficacy of MNK/eIF4E and mTORC1 co-targeting but is likely instead to rely on reduced translation of specific transcripts. We therefore sought to identify the mRNAs bound by total eIF4E and P-eIF4E by RNA immunoprecipitation (RIP) from APC KRAS organoids. Immunoblotting samples from these RIPs shows the enrichment for P-eIF4E and the recovery of total eIF4E (both phosphorylated and non-phosphorylated forms) from parallel eIF4E RIPs (Figure 5A). qPCR of RNA purified from these RIPs reveals uniform binding of transcripts by total eIF4E between predicted ‘P-eIF4E-dependent’ and control mRNAs (Figure 5B)(20,22,23). qPCR from P-eIF4E RIPs shows an enrichment for ‘P-eIF4E dependent’ messages when compared to control transcripts *ActB* and *Gapdh* with the *C-myc* transcript significantly enriching in P-eIF4E RIPs compared to the *Gapdh* transcript (Figure 5B). Similarly, RIPs performed using exogenous Flag-eIF4E expressed in HCT116 cells found a significant enrichment of *c-MYC*, among other P-eIF4E dependent transcripts, than control *TUBA1B* transcript (Figure S5G). Importantly, expression of Flag-eIF4E mutated with the S209A mutation reduced the enrichment for *c-*

MYC over control transcripts (Figure S5G). This indicates that Flag-eIF4E that can be phosphorylated associates more readily with *c-MYC* than non-phosphorylatable Flag-eIF4E.

C-myc has particular pertinence in CRC, demonstrated by the effects of its deletion in *Apc*-deficient GEMMs (40). We analyzed the expression of nuclear c-MYC in colonic adenomas from APC KRAS MNK1/2 KO tumor model mice treated with or without rapamycin compared to APC KRAS mice. Nuclear c-MYC expression was decreased in adenomas from APC KRAS MNK1/2 KOs treated with rapamycin (Figure 5C) but relatively unchanged in the corresponding short-term model (Figure S5H). Cytoplasmic c-MYC expression followed a similar pattern, but at less than half the levels of nuclear c-MYC (Figure S5I). Western blotting of lysates from APC KRAS MNK1/2 KOs organoids also showed a consistent reduction in c-MYC expression following rapamycin treatment (Figure S5J). Importantly, *C-myc* mRNA expression was not altered by the presence or absence of the MNKs or rapamycin treatment (Figure S5K). Therefore, P-eIF4E is enriched on *C-myc* mRNAs and, when this pathway is suppressed in conjunction with rapamycin treatment, the expression of c-MYC falls.

Co-targeting of MNK and mTORC1 suppresses KRAS-driven tumorigenesis

We next sought to recapitulate our genetic data with small molecule inhibitors. To inhibit the MNKs, we used the potent MNK inhibitor eFT508 (24,26). eFT508 treatment of the APC KRAS short-term model substantially reduced P-eIF4E but had little effect on proliferation (Figures 6A and S6A). Combination of eFT508 with rapamycin significantly reduced proliferation, compared to animals treated with both vehicles, (Figure 6A), to a level similar to APC KRAS MNK1/2 KOs treated with rapamycin (Figure 4E). eFT508 was present at over 3nM in the plasma and 300nM in the intestine 2hours after oral gavage, concentrations which were not altered by concurrent dosing with rapamycin (Figure S6B). A similar effect was seen targeting the MNKs with the multi-kinase inhibitor merestinib (Figure S6C). Drug combination efficacy was independent of signaling to eEF2 via eEF2K, as shown by suppressed proliferation in eFT508/rapamycin or merestinib/rapamycin combinations in $VillinCre^{ER}$ $Apc^{fl/fl}$ $Kras^{G12D/+}$ $eEF2K^{D273A/D273A}$ intestines (Figures S6C and S6D)(41). When analyzed in the elongation-dependent APC model, this eEF2K inactivating allele completely removes sensitivity to rapamycin (Figure S6E). This confirms that rapamycin (and MNK inhibition) do not reduce proliferation via eEF2K-dependent slowing of elongation. Combination of rapamycin and eFT508 in this APC model (with wild-type *Kras*) had no additional effect on proliferation than rapamycin treatment alone (Figure S6E).

eFT508/rapamycin was effective in the APC KRAS tumor model, significantly suppressing proliferation after 5days of treatment, with a reduction in P-eIF4E (Figures 6B and 6C). Suppression of proliferation by eFT508/rapamycin in APC KRAS adenomas correlated with reduced nuclear and cytoplasmic c-MYC expression (Figures 6C, 6D and S6F). APC KRAS organoids treated with the combination for 24hours also had reduced c-MYC expression (Figure S6G). Treatment of mice bearing adenomas also significantly extended survival, with animals living up to 120days on treatment, compared with less than 10days with vehicle treatment (Figure 6E). Combination treatment was extremely well tolerated, with excellent biomarker modulation but no adverse effects on homeostasis in wild-type mice

(Figure S6H). c-MYC expression was also unaltered by combination treatment in wild-type mice, indicating that this modulation is specific to the APC KRAS tumor model, and not a wider effect on c-MYC expression. Treatment of the orthotopic APC KRAS colonic polyp model with eFT508/rapamycin resulted in a similar extension of survival when compared with the single drug treatments (Figure S6I) and treatment of APC KRAS organoids with rapamycin and eFT508 in combination reduced cell metabolic activity, a surrogate for cell number, by ~40% (Figures 6F and S6J).

Mechanistically, eFT508 treatment was similar to *Mnk* knockout. eFT508 suppressed protein synthesis, with no additive inhibition when combined with rapamycin (Figure S6K). Of note, RIPs performed following eFT508 treatment of APC KRAS organoids showed no change in the quantity of *C-myc* bound by total eIF4E (Figure S6L). Thus, P-eIF4E does not increase the recruitment of eIF4E to mRNAs, consistent with previous reports (27,42), but likely promotes translation transcripts when bound.

The efficacy of MNKi and rapamycin is entirely dependent upon regulation of c-MYC

Targeting P-eIF4E in combination with rapamycin treatment, consistently results in a reduction in nuclear c-MYC protein expression (Figures 5C and 6D). However, it is unclear whether this is a cause or consequence of reduced proliferation. To test this, we used an inducible human *C-MYC* cDNA lacking 5′- or 3′-UTRs preceded by a Cre-activated LoxP-STOP-LoxP (lsl) cassette in the *Rosa26* locus (*R26-lsl-MYC*) (43). Following recombination, two additional copies of c-MYC are expressed in the intestinal epithelium concomitant with *Apc* deletion and $KRAS^{G12D}$ activation. These mice are referred to as APC KRAS MYC.

The expression of additional c-MYC had little effect on proliferation in established adenomas (Figure 7A), with similar nuclear levels of c-MYC between untreated APC KRAS and APC KRAS MYC ageing model mice (Figure 7B). However, proliferation in adenomas of these APC KRAS MYC mice was unaffected by treatment with eFT508/rapamycin, in contrast with the almost 50% reduction in proliferation in treated APC KRAS adenomas (Figure 7A). In line with sustained proliferation, treated APC KRAS MYC adenomas showed higher expression of nuclear c-MYC compared to treated APC KRAS adenomas (Figure 7B). APC KRAS MYC organoids also showed increased average expression of c-MYC following eFT508/rapamycin treatment compared with APC KRAS organoids (Figure S6G). Cytoplasmic c-MYC follows the same pattern (Figure S7A). Furthermore, the extension of survival seen with eFT508/rapamycin in APC KRAS tumor model mice (median 49days) was completely lost in APC KRAS MYC mice (median <4days) (Figure S7B), despite eFT508 suppressing P-eIF4E to a similar extent (Figure S7C). The *C-MYC* transgene produced similar results in the APC KRAS short-term model (Figure 7C) and organoid culture (Figure 7D) with proliferation comparable between APC KRAS MYC mice or organoids treated with eFT508/rapamycin and vehicle-treated APC KRAS. Altogether, these data reveal that the suppression of c-MYC protein expression by eFT508/rapamycin entirely accounts for the reduction in proliferation in the APC KRAS model.

eFT508/rapamycin treatment suppressed protein synthesis in APC KRAS MYC cells to a similar extent as APC KRAS organoids (Figure S7D). Thus, the re-expression of c-MYC

does not drive proliferation by simply restoring protein synthesis. We hypothesize that rapamycin acts to suppress global protein synthesis, creating a requirement for P-eIF4E to promote c-MYC expression. To test this we used three therapeutically relevant agents that suppress global protein synthesis, oxaliplatin, 5-fluorouracil (5FU), and rocaglamide (44–46), in the place of rapamycin, finding that APC KRAS organoids were sensitized to treatment with these compounds by co-administration of eFT508 (Figure S7E). This sensitization was dependent on suppression of c-MYC as APC KRAS MYC organoids were refractory to eFT508 combination treatment. Thus, MNK inhibition acts to suppress proliferation in tumor cells where protein synthesis is limiting, by suppressing c-MYC expression.

c-MYC restores proliferation by altering transcription of metabolic genes

The c-MYC transgene is unable to restore protein synthesis rates following eFT508/rapamycin treatment, even after 1 week of exposure to the compounds in culture (Figure S7F). We therefore investigated how c-MYC is restoring proliferation by performing an RNAseq analysis from APC KRAS and APC KRAS MYC whole intestines, treated with or without eFT508/rapamycin. This revealed few changes in mRNA abundance (68 altered transcripts) following c-MYC expression in the absence of treatment but comparing APC KRAS and APC KRAS MYC intestines treated with the combination revealed 335 altered transcripts (154 up, 181 down) (Figure S7G). Of these transcripts only 9 were altered by expression of the transgene in the absence of drug treatment. REACTOME and Gene Set Enrichment Analysis revealed that the transcripts upregulated by c-MYC regulate metabolic pathways such as oxidative phosphorylation and arachidonic acid metabolism (47,48) (Figures 7E and S7H). There was no enrichment for changes in canonical c-MYC-modulated transcripts, such as ribosomal constituents or RNA polymerases. Transcriptional upregulation of specific metabolism-linked transcripts was confirmed by qPCR from intestinal tissue as well as organoids treated with eFT508/rapamycin for one week (Figures S7F and S7I). Interestingly, the c-MYC transgene does not revert gene expression to resemble untreated control APC KRAS intestines, as evidenced by 865 differently expressed transcripts (573 up, 295 down) when comparing these two conditions (Figure S7G). Thus, the c-MYC transgene specifically drives a transcriptional program focusing on metabolism only following eFT508/rapamycin treatment, which likely enables proliferation to be restored. This analysis will provide insight into c-MYC-driven resistance mechanisms, identifying oxidative phosphorylation and arachidonic acid metabolism as potential targets. c-MYC regulation of arachidonic acid metabolism has previously been seen in *Kras*-mutant mouse models of lung cancer (49) and the arachidonic acid pathway is pro-tumorigenic in preclinical models of CRC, with inhibitors such as celecoxib proving to be clinically effective preventative therapies (50).

Given the efficacy of targeting the MNKs in combination with rapamycin in the APC KRAS model, we applied this treatment to more complex mouse models of CRC, bearing further mutations prevalent in the human disease. For this, we used APC KRAS organoids also lacking *Tp53* and *Tgfbr1*, termed *AKPT* (*VillinCre*^{ER} *Apc*$^{fl/fl}$ *Kras*$^{G12D/+}$ *Tp53*$^{fl/fl}$ *Trgfbr1*$^{fl/fl}$), and organoids isolated from liver metastases from the *KPN* autochthonous CRC model (*VillinCre*^{ER} *Kras*$^{G12D/+}$ *Tp53*$^{fl/fl}$ *R26*^{N1ICD}) (51). In both cases, eFT508/rapamycin

Europe PMC Funders Author Manuscripts

significantly suppressed proliferation (Figures S7J), expanding the efficacy of the treatment combination to include additional cancer mutations.

Elevated MNK and mTORC1 signaling predicts poor survival

Next, we investigated the translatability of dual MNK and mTORC1 targeting in patients with CRC. Thus, we analyzed patient survival in relation to P-eIF4E and P-RPS6 and treated organoids from CRC patients with MNK and mTORC1 inhibitors. Neither P-eIF4E and P-RPS6 alone associated with survival in the full cohort of CRC patients analyzed (Figure S7K). However, when stratified by GMS, P-RPS6 levels were significantly associated with poor cancer-specific survival in GMS1 patients (tumors with low inflammatory infiltrate and low tumor-stroma percentage) (Figure S7K). GMS1 tumors are highly epithelial, predicted to be the least likely to respond to immunotherapy and often have few therapeutic options. The pre-clinical mouse models we have used present with highly epithelial tumors, correlating well with GMS1 tumors. P-RPS6 and P-eIF4E positively correlate in these clinical samples, and our animal data predicts a synergy between the two pathways to promote proliferation. We therefore combined the two markers into a single score, comparing survival of patients with tumors exhibiting low phosphorylation of one or both with patients with high phosphorylation of both markers. GMS1 patients with high MNK and mTORC1 signaling had a significantly worse prognosis than those with low expression(s) (Figure 7F). Indeed, mean cancer specific survival of ‘both high’ patients was more than 3.5 years shorter than ‘one or both low’ patients. These ‘both high’ GMS1 patients with poor survival accounted for 1 in 5 of the patients in the TMA. Across the full cohort signaling through both pathways had no significant advantage, illustrating the specificity to GMS1 tumors (Figure S7K).

Finally, we applied MNK and mTORC1 inhibitors to two patient-derived organoid lines bearing deletion of *APC* and $KRAS^{G12D}$ mutations (52). These organoids faithfully recapitulate patient response to treatments, providing an excellent system for the discovery of clinically translatable therapeutics. Both organoid lines were refractory to rapamycin treatment but responded to eFT508/rapamycin combination with a 20% reduction in Cell-Titer Blue activity after 24h (Figure S7L). 30nM eFT508 completely suppressed P-eIF4E in these human organoids, and combination treatment resulted in reduced c-MYC expression in one of the lines (Figure S7M). Consistent with the effect of eFT508 in these human organoids, treatment with merestinib reduced proliferation in combination with rapamycin in both lines (Figure S7L). Altogether, the successful co-targeting of mTORC1 and the MNK/eIF4E pathway used in our pre-clinical mouse models has excellent potential to translate to the clinic where we see heightened mTORC1 and MNK signaling correlate with poor survival in a population of CRC patients.

Discussion

Although G12C mutants may now be targetable, these only occur 3% of all CRC (4), meaning that most *KRAS*-mutant CRCs lack effective clinical options. To address this, we sought to target protein synthesis. We show that activation of KRAS in the mouse intestine increases protein synthesis, conferring resistance to rapamycin, consistent with resistance to

rapalogs in the clinic (7–9). We show that the mode of action of rapamycin is altered by *Kras* mutation, with translation elongation unaffected but translation initiation suppressed. Our data also reveal uncoupling of protein synthesis and proliferation, with reduced translation in our APC KRAS model in response to rapamycin but no effect on proliferation. We go on to show that signaling pathways regulating the translation machinery are viable targets in *KRAS*-mutant CRC by inhibiting P-eIF4E in combination with rapamycin, which reduces proliferation in multiple CRC GEMMs. This combination suppressed expression of c-MYC, compromising tumor proliferation, with expression of a human *C-MYC* transgene completely reversing the benefit of treatment. c-MYC expression from the transgene is within the physiological range with little-to-no difference in c-MYC levels between adenomas from APC KRAS and APC KRAS MYC tumor model mice. We attribute this to excessive expression of c-MYC being restrained to protect against MYC-induced apoptosis (53).

Within APC KRAS cells, c-MYC expression is maintained by high protein synthesis rates and P-eIF4E. Reducing protein synthesis using rapamycin is tolerated by tumors due to P-eIF4E maintaining c-MYC levels. Similarly, targeting P-eIF4E alone does not suppress c-MYC expression likely due to the continued translation capacity. However, reducing protein synthesis and inhibiting P-eIF4E result in decreased c-MYC expression and less proliferation. Inhibition of either mTORC1 or the MNKs has previously been implicated in regulation of *C-MYC* translation (23,54–56) and combination targeting has previously been shown to suppress IRES-dependent translation of c-MYC (57). It is noteworthy that the human *C-MYC* transgene used here lacks a 5′-UTR and therefore an IRES, providing an avenue for future investigation into the mechanism behind eFT508/rapamycin-dependent suppression of c-MYC. Expression of c-MYC protein is restrained by the eIF2B complex in the same CRC mouse models used here, with depletion of eIF2B5 resulting in increased c-MYC expression and MYC-dependent apoptosis (58). This highlights the importance of translation in determining c-MYC expression in CRC and, together with our work, positions c-MYC modulation downstream of targeting of protein synthesis.

The co-targeting of the MNKs and mTORC1, or other kinases, reduces proliferation or colony formation in cell lines from a variety of cancers (20,38,39,59–63). We provide the first evidence for efficacy of this drug combination in a pre-clinical *in vivo* model. The mode of action of this drug combination was not fully elucidated in these previous studies; data within some are consistent with our observations that targeting of the MNKs and mTORC1 converges on translation initiation and are consistent with MNK deletion or inhibition suppressing global protein synthesis (20,38,39). eFT508 (Tomivosertib) is in phase II clinical trials in combination with checkpoint inhibitors against solid tumors including CRC, and with paclitaxel in breast cancer. The efficacy of eFT508/rapamycin to suppress proliferation and extend survival of mice by over 20-fold shown here is encouraging as a potential therapy for *KRAS*-mutant CRC patients. The combination is also effective in patient-derived CRC organoids that faithfully recapitulate drug responses. We also identify a population of CRC patients (>45%) with co-occurrence of high mTORC1 and MNK signaling and observed that patients with highly epithelial tumors fare significantly worse when these pathways are activated.

In our models, signaling through the MNKs drives cancer cell proliferation in a cell-intrinsic manner. MNK inhibition also suppresses neutrophil activation in response to multiple stimuli (64), inhibits TNFα production in T cells (65), and, in a breast cancer model, eIF4E KI mice have fewer pro-metastatic neutrophils and metastases (66). P-eIF4E also has a cancer cell-intrinsic role in promoting PD-L1 expression in a *Kras*-mutant model of hepatocellular carcinoma (24). Targeting P-eIF4E, using eFT508, reduced PD-L1 levels and attenuated primary tumor growth and metastasis. It is possible there will be an additional benefit of targeting both tumor cell proliferation and immune cell activity via P-eIF4E.

We see high P-eIF4E in ~70% of patients, in agreement with a previous study where P-eIF4E was seen in ~60% of human CRC samples (67). As well as CRC, P-eIF4E is increased in head and neck squamous cell carcinoma (HNSCC) and lung cancer (67). Lung adenocarcinomas exhibit mutations in *KRAS*, and HNSCCs exhibit mutations in its paralogue *HRAS* (68)(69), with MYC expression also important in both tumor types. The successful therapeutic regimen used here may be of benefit to patients with *RAS*-mutant cancers that present with elevated levels of P-eIF4E and a reliance on MYC expression. This work opens the possibility to address oncogenic *RAS* signaling across many tumor types by targeting its downstream regulators of mRNA translation.

Methods

Materials availability

All mouse strains are, where possible, available on request, but may be subject to payment and/or a Materials Transfer Agreement.

Clinical studies

This study was approved by the West of Scotland Research Ethics Committee (16/WS/0207) and patient information is held within the Greater Glasgow and Clyde Safe Haven (12/WS/0142). The TMA used four 0.6mm cores per patient. Tumor staging used the 5th Edition of the AJCC/UICC-TNM system. GMS was constructed by combining a tumor-stromal percentage and the Klintrup-Mäkinen scores as previously described (11). 192 stage I-III patients that underwent curative CRC tumor resection surgery in Glasgow Royal Infirmary, Western Infirmary, or Stobhill Hospitals (Glasgow, UK) between 1997 and 2007 were included in the study. Patients who died within 30days of surgery or underwent neo-adjuvant therapy were excluded. Patients were followed for at least five years post resection, with 49 cancer deaths. All had valid scores for P-RPS6 S240/4 and 191 for P-eIF4E S209. The TMA was stained using a duplex chromogenic immunohistochemistry (IHC) method on a Ventana Discovery Ultra autostainer (Roche) using Ventana reagents and detection systems and the following antibodies; P-RPS6 S240/4 (Cell Signaling Technology (CST) 5364), P-eIF4E S209 (Abcam ab76256) and cytokeratin (Leica AE1/AE3-L-CE). Slides were imaged on a Hamamatsu Nanozoomer XR and analyzed using Visiopharm version 2019.02.2.6239. To outline tumor regions a supervised K-means clustering app was developed. A decision forest app was developed to detect cells within tumors and cytoplasmic staining was binned by intensity to calculate a H-Score. ROC curves were constructed in MEDCalC and Youden's J index employed to determine the cut-off between high and low staining for both antibodies.

Europe PMC Funders Author Manuscripts

Mouse studies

Experiments were performed under license from the UK Home Office (60/4183 and 70/8646). Mice were genotyped by Transnetyx (Cordova, Tennessee). All colonies were inbred C57BL/6J (Generation ≥7), except those with the *eIF4E*^{S209A} or *Rosa26-lsl-MYC* alleles, which were outbred. Mice were housed in conventional cages with a 12-hour light/dark cycle and *ad libitum* access to diet and water. Experiments were performed on males and females between 6 and 12 weeks old. Researchers were not blinded. Sample sizes are shown in the figures or legends. *Villin*^{CreER} mediated recombination was induced by intraperitoneal (IP) injection of tamoxifen dissolved in corn oil at 80mg/kg (70). For orthotopic inductions, 70μL of 100nM 4-OH tamoxifen was injected into the colonic submucosa using a TelePack VetX LED endoscope (Karl Storz)(36). Tumor model experiments were initiated by single dose of tamoxifen on day 0, mice monitored until signs of intestinal disease – weight loss, paling feet from anemia and hunching behavior. For treatment when sick experiments, these were initiated when mice had lost >3% of their stable weight. Mice were sequentially recruited onto vehicle or drug treatment to ensure no bias and equal cohort sizes. Tumors were scored macroscopically after fixation of opened intestinal tissue. For short-term experiments, mice wild-type for *Kras* were induced on consecutive days (0 and 1) and subsequently sampled on day4. Mice bearing the *Kras*^{G12D} allele were induced with a single injection of tamoxifen and sampled on day 3 post-induction. Animals were split into drug treatment groups randomly, ensuring equal gender separation between cohorts. Rapamycin (LC Laboratories R-5000) was dosed by daily IP at 10mg/kg (5). Merestinib (Axon MedChem 2553) was suspended in 10% gum Arabic and dosed at 12mg/kg by daily oral gavage (OG)(23). eFT508 (manufactured in house) was suspended in 1% methylcellulose, 0.15% Tween-80 and dosed twice daily at 1mg/kg by OG. 250μL of BrdU cell proliferation labelling reagent (Amersham Bioscience RPN201) was administered by IP 2hours prior to sampling.

Histology and immunohistochemistry

Tissue was fixed in formalin and embedded in paraffin. IHC was carried out as previously (5), using the following antibodies P-eIF4E S209 (Millipore 04-1058), RPS6 P-S240/4 (CST 5364), P-4E-BP1 (CST 2855), P-eEF2 T56 (Novus Biologicals NB100-92518), BrdU (BD Biosciences 347580), P-eIF4B S422 (AbCam ab59300), c-MYC (Santa Cruz Biotechnology Sc-764) and RFP (Tebu Bio 600-401-379). A minimum of 3 biological replicates were analyzed and representative images displayed. For BrdU scoring in short-term model experiments tissue was fixed in methanol:choloform:acetic acid at a ratio 4:2:1, transferred to formalin and embedded in paraffin. For BrdU scoring in the tumor model, formalin-fixed paraffin-embedded tissue was analyzed using Halo Software, trained to quantify BrdU-positive nuclei in epithelial tumor cells as a percentage of all epithelial tumor cells. BaseScope analysis was carried out according to the manufacturers guidelines (ACD) using custom probes to murine *Mnk1* bases 658-789 and *Mnk2* bases 727-888.

Cell culture

Organoid cultures were isolated and maintained in Matrigel (Corning 356231). Advanced DMEM/F12 media (Life Technologies 12634-028) was supplemented with 5mM HEPES

(Life Technologies 15630-080), 2mM L-glutamine (Life Technologies 25030-024), 100U/mL penicillin/streptomycin (Life Technologies 1540-122), 1x N2 (Invitrogen 17502-048), 1x B27 (Invitrogen 12587-010), 100ng/mL noggin (Peprotech 250-38) and 50ng/mL EGF (Peprotech AF-100-15). Patient derived organoids were grown in the same media supplemented with 500ng/mL R-spondin (R&D Systems 3474-RS) 10nM gastrin (Sigma Aldrich G9145), 100ng/mL Wnt-3A (R&D Systems 5036-WN), 10μM Y-27632 (Sigma Aldrich Y0503), 0.5μM A83-01 (Peprotech 2939), 5μM SB202190 (Sigma Aldrich S7067), 4mM nicotinamide (Sigma Aldrich N0636), 10ng/mL FGF basic (Peprotech 100-18B), 10ng/mL FGF10 (Peprotech 100-26A), 1μM prostaglandin E2 (Peprotech 2296). For cell proliferation assays, cells were plated in 96 well-plates, established for 2-3days before using Cell-Titer Blue to measure metabolic capacity as a surrogate for cell number (Promega G8080). Drugs (5FU (Mayne Pharma Plc PL04515/0088), Oxaliplatin (Acoord Healthcare Ltd PL20075/0112) and rocaglamide (Sigma Aldrich SML0656)) were dosed for 24hours prior to addition of Cell-Titer Blue for the final 2-6hours. Changes in metabolic capacity were normalized to vehicle treated cells. All experiments with organoids were performed before passage 20. HCT116 cells were cultures in DMEM supplemented with 2mM L-glutamine and 10% FBS (Life Technologies). Testing of lines for mycoplasma was performed using MycoAlert (Lonza LT07-218).

RNA immunoprecipitation

Organoids were harvested in ice-cold PBS and Matrigel and washed in ice-cold PBS. Lysis was in RNA immunoprecipitation (RIP) buffer (20mM Tris-HCL pH 7.5, 200mM NaCl, 5mM MgCl2, 0.5% Triton X-100, protease inhibitor cocktail (Roche 11836153001), 800U RiboLock RNase inhibitor (Thermo Fisher Scientific (TFS) EO0381), 10% BSA, 0.5μM DTT, 5μM NaF) and aided by 8x passages through a 21-gauge needle. Lysates were centrifuged, supernatant protein concentration determined, and an equal concentration used for each RIP. In addition, samples were collected for RNA and protein extraction. Antibodies, IgG control (CST 2729), eIF4E (TFS MA1089), and P-eIF4E S209 (Abcam ab76256), were incubated with Dynabeads Protein G (TFS 10004D) for 2.5hours. The affinity purification was conducted for 30minutes at 4°C with constant rotation, before washing 3x with RIP buffer. The resulting elution was split for protein or RNA extraction by Trizol (TFS 10296010). RNA integrity was assessed by RNA ScreenTape (Agilent Technologies 5067-5576) on 4200 TapeStation System. Flag-eIF4E constructs were generated by amplifying human eIF4E from Addgene plasmid #17343 using 5′-CTGGAGATCTGATGGCGACTGTCGAACCGGAAACCAC-3′ and 5′-GCGTGGATCCTTAAACAACAAACCTATTTTTAGTGGTGGAGC-3′, digesting with *BglII* and *BamHI* and ligating into p3x-FLAG-CMV vector (Sigma Aldrich E7533). S209A mutation was achieved by site directed mutagenesis using QuikChange Lightning (Agilent 210518) and the following primers 5′-CGCAGACAGCTACTAAGAGCGGCGCCACCACTAAAAATAG-3′ and 5′-CTATTTTTAGTGGTGGCGCCGCTCTTAGTAGCTGTCTGCG-3′. Plasmids were transfected into HCT116 cells using Lipofectamine 2000 (TFS 11668019) as per manufacturer's instructions. 24hours post-transfection 30million cells per condition were harvested by trypsinization. This was lysed in RIP buffer then the cleared lysates mixed with pre-washed anit-Flag antibody conjugated beads (Merck M8823) for 30mins at 4°C, washed

then RNA eluted in Trizol. Parallel input samples were retained, and RNA also purified by Trizol. p3xFLAG-BAP control plasmid was supplied by Sigma Aldrich.

qPCR

RNA was purified from tissue by RNeasy (Qiagen 74104) following disruption in CK14 Precellys tubes with on-column DNAse digestion. Purified RNA was reverse transcribed (Superscript III) using random hexamers and qPCR performed using the following primers for murine transcripts. *Mnk1*: Fd 5′-CCATCGTGGATTCTGACAAGAG-3′, Rv 5′-GAACACTCGACTTCGACTGTG-3′. *Mnk2*: Fd 5′-TCGGGCTACTGACAGCTTCT-3′, Rv 5′-GACACAGGTCTGCACACGAG-3′. *C-myc*: Fd 5′-CCCAAATCCTGTACCTCGTC-3′, Rv 5′-TTGCCTCTTCTCCACAGACA-3′. *ActB*: Fd 5′-GTGACGTTGACATCCGTAAAGA-3′, Rv 5′-GCCGGACTCATCGTACTCC-3′. *Cyclin D1*: Fd 5′-GAGAAGTTGTGCATCTACACTG-3′. Rv 5′-AAATGAACTTCACATCTGTGGC-3′. *Cyclin E*: Fd 5′-GTGGCTCCGACCTTTCAGTC-3′ Rv 5′-CACAGTCTTGTCAATCTTGGCA-3′. *Mcl1*: Fd 5′-GACGACCTATACCGCCAGTC-3′ Rv 5′-AGAGGCTTCGAGTCCTTGGA-3′. *Snail1*: Fd 5′-CACACGCTGCCTTGTGTCT-3′ Rv 5′-GGTCAGCAAAAGCACGGTT-3′. *Runx2*: Fd 5′-AGAGTCAGATTACAGATCCCAGG-3′ Rv 5′-TGGCTCTTCTTACTGAGAGAGG-3′. *Gapdh*: Fd 5′-TCCACTGGCGTCTTCACC-3′ Rv 5′-GGCAGAGATGATGACCCTT -3′. *Enpp7:* Fd 5′-GACAGCATAAGCTACTCCTCGT-3′ Rv 5′-GACAGCATAAGCTACTCCTCGT-3′. *Slc36a1*: Fd 5′-GACTACAGTTCCACAGACGTG-3′ Rv 5′-CCATGTCATGCTACTGCTCTCT-3′. *Car4*: Fd 5′-TACGTGGCCCCCTCTACTG-3′ Rv 5′-GCTGATTCTCCTTACAGGCTCC-3′ These primers were used for human transcripts: *c-MYC*: Fd 5′-TACAACACCCGAGCAAGGAC-3′ Rv Fd 5′-GAGGCTGCTGGTTTTCCACT-3′. *Cyclin D1*: Fd 5′-GAGAAGTTGTGCATCTACACTG-3′. Rv 5′-AAATGAACTTCACATCTGTGGC-3′. *Cyclin E:* Fd 5′-ACTCAACGTGCAAGCCTCG-3′ Rv 5′-GCTCAAGAAAGTGCTGATCCC-3′. *MCL1:* Fd 5′-GCTCAAGAAAGTGCTGATCCC-3′ Rv 5′-TAGCCACAAAGGCACCAAAAG-3′. *ACTB*: 5′-GCCAACAGAGAGAAGATGAC-3′ Rv 5′-CGCAAGATTCCATACCCAGG-3′. *TUBA1B*: Fd 5′-AGCATCCAGTTTGTGGATTGGTGC-3′ and Rv 5′-CAAAGGCACGCTTGGCATACATCA-3′. *GAPDH*: Fd 5′-CTATAAATTGAGCCCGCAGCC-3′ Rv Fd 5′-ACCAAATCCGTTGACTCCGA-3′.

RNA sequencing

Libraries for cluster generation and DNA sequencing were prepared following a previously described method (71) using a TruSeq RNA sample prep kit v2 (Illumina), then run on an Illumina NextSeq using the High Output 75 cycles kit (2x36 cycles, paired end reads, single index). Raw sequence quality was assessed using FastQC version 0.11.8, then sequences were trimmed to remove adaptor sequences and low-quality base calls, defined as those with a Phred score of less than 20, using Trim Galore version 0.6.4. Trimmed sequences were aligned to mouse genome build GRCm38.98 using HISAT2 version 2.1.0 and raw counts per gene were determined using FeatureCounts version 1.6.4. Differential expression analysis was performed using the R package DESeq2 version 1.22.2, then pathway analysis was

performed on significantly changed genes (defined as FDR <0.05) using the R package ReactomePA version 1.26.0. The data discussed in this publication have been deposited in NCBI's Gene Expression Omnibus, accessible through GEO Series accession number GSE159432.

Western blotting

Samples were lysed (10mM Tris (pH 7.5), 50mM NaCl, 0.5% NP40, 0.5% SDS supplemented with protease inhibitor cocktail, PhosSTOP (Roche 04906837001) and benzonase (Sigma Aldrich E1014) on ice and protein quantity estimated by BCA assay (TFS 23225). 20μg of protein were denatured in SDS loading dye then resolved by 4-12% SDS-PAGE (Invitrogen NP0336BOX). Protein was transferred to nitrocellulose and immunoblotted overnight at 4°C using the following antibodies; eIF4E (CST 2067), P-eIF4E S209 (CST 9741), RPS6 (CST 2317) RPS6 P-S240/4 (CST 5364), 4E-BP1 (CST 9644), eEF2 (CST 2332), P-eEF2 T56 (CST 2331), eIF4B (CST 3592), P-eIF4B S422 (CST 3591), eIF4G1 (CST 2498), P-eIF4G1 S1108 (CST 2441), FLAG (Abcam ab1162), vinculin (ab18058 Abcam), and β-actin (Sigma Aldrich A2228). HRP-conjugated secondary antibodies (Dako P0447, P0448) were incubated for 1 hour at room temperature then membranes were exposed to autoradiography films in ECL (TFS 32106). Quantification was performed using Image J (NIH).

Sucrose density gradients

Organoids were replenished with medium for 6hours then medium spiked with 200μg/mL cycloheximide (Sigma Aldrich C7692) 3minutes prior to harvesting on ice. Crypt fractions were isolated by epithelial extraction from 10cm of proximal small intestine. Villi were removed by incubating PBS-flushed linearly opened intestines in RPMI media (TFS 21875059) supplemented with 10mM EDTA and 200μg/mL cycloheximide for 7minutes at 37°C with regular agitation. Crypts were then isolated by transferring tissue to ice-cold PBS containing 10mM EDTA and 200μg/mL cycloheximide for 7minutes. The remaining tissue was then discarded. Samples were lysed (300mM NaCl, 15mM $MgCl_2$, 15mM Tris pH 7.5, 100μg/mL cycloheximide, 0.1% Triton X-100, 2mM DTT and 5U/mL SUPERaseIn (TFS AM2696)) on ice and post-nuclear extracts layered on 10-50% weight/volume sucrose gradients containing the same buffer with no Triton X-100, DTT, or SUPERaseIn. Gradients were spun at 255,000rcf for 2hours at 4°C under a vacuum in an SW40Ti rotor. After centrifugation, samples were separated through a 254nM optical density reader (ISCO). Polysome to subpolysome (P:S) ratios were calculated using the trapezoid method with the boundaries defined manually. For harringtonine run-off analyses, cultures were prepared in duplicate, one pretreated with 2μg/mL harringtonine (Santa Cruz Biotechnology sc-204771) for 5minutes (300seconds) prior to cycloheximide addition, then both processed as above. Run-off rates were calculated as the P:S ratio without harringtonine over the P:S ratio with harringtonine.

^{35}S-methionine labelling

Organoids were analyzed during optimal growth phase, 3days after splitting, and 6hours after a media change. ^{35}S-methionine (Perkin Elmer NEG772002MC) was spiked at 30μCi/mL for 30minutes prior to harvesting and lysed using the western blotting buffer.

Europe PMC Funders Author Manuscripts

Protein was precipitated in 12.5% (w/v) trichloroacetic acid onto glass microfiber paper (Whatmann 1827-024) using a vacuum manifold and washed with 70% ethanol and acetone. Scintillation was read on a Wallac MicroBeta TriLux 1450 counter using Ecoscint (SLS Ltd LS271) and normalized to total protein content determined by the BCA assay. Protein synthesis rate was expressed as scintillation over protein content (CPM / μg/mL protein) relative to a control sample set to 1.

Statistical analysis

Statistical analyses and n numbers are outlined in each Figure or its legend. In all cases, *P* values equal to or less than 0.05 were considered significant.

Supplementary Material

Refer to Web version on PubMed Central for supplementary material.

Acknowledgements

Funding for the Sansom laboratory was from CRUK (A17196, A24388, A21139), The European Research Council ColonCan (311301), a Wellcome Trust Collaborative Award in Science (201487) and a CRUK Grand Challenges (A25045 and A29055). JDL was supported by an MRC Clinical Research Predoctoral Training Fellowship (MR/N021800/1). KP was supported by an MRC Fellowship (MR/R502327/1). The authors are grateful to the Core Services and Advanced Technologies at the CRUK Beatson Institute (C596/A17196), particularly the Histology Services, Transgenic Technology Laboratory, Molecular Technologies and Biological Services Unit. We thank Michael Pollak from McGill University for critical reading of the manuscript.

References

1. Guinney, J, Dienstmann, R, Wang, X, de Reynies, A, Schlicker, A, Soneson, C. , et al. Nat Med. Vol. 21. United States: 2015. The consensus molecular subtypes of colorectal cancer; 1350–6.
2. Yaeger, R, Chatila, WK, Lipsyc, MD, Hechtman, JF, Cercek, A, Sanchez-Vega, F. , et al. Cancer Cell. Vol. 33. Elsevier; 2018. Clinical Sequencing Defines the Genomic Landscape of Metastatic Colorectal Cancer; 125–136. Available from [Internet]
3. DeStefanis RA, Kratz JD, Emmerich PB, Deming DA. Targeted Therapy in Metastatic Colorectal Cancer: Current Standards and Novel Agents in Review. Curr Colorectal Cancer Rep. 2019; 15:61–9. DOI: 10.1007/s11888-019-00430-6 [PubMed: 31130830]
4. Hong, DS, Fakih, MG, Strickler, JH, Desai, J, Durm, GA, Shapiro, GI. , et al. N Engl J Med. Vol. 383. Massachusetts Medical Society; 2020. KRASG12C Inhibition with Sotorasib in Advanced Solid Tumors; 1207–17. Available from [Internet]
5. Faller WJ, Jackson TJ, Knight JRP, Ridgway RA, Jamieson T, Karim SA, et al. MTORC1-mediated translational elongation limits intestinal tumour initiation and growth. Nature. 2015; 517
6. Yuksekkaya, H, Yucel, A, Gumus, M, Esen, H, Toy, H. Am J Gastroenterol. United States: 2016. Familial Adenomatous Polyposis; Succesful Use of Sirolimus; 1040–1.
7. Ng K, Tabernero J, Hwang J, Bajetta E, Sharma S, Del Prete SA, et al. Phase II study of everolimus in patients with metastatic colorectal adenocarcinoma previously treated with bevacizumab-, fluoropyrimidine-, oxaliplatin-, and irinotecan-based regimens. Clin Cancer Res. 2013; 19:3987–95. [PubMed: 23743569]
8. Spindler K-LG, Sorensen MM, Pallisgaard N, Andersen RF, Havelund BM, Ploen J, et al. Phase II trial of temsirolimus alone and in combination with irinotecan for KRAS mutant metastatic colorectal cancer: outcome and results of KRAS mutational analysis in plasma. Acta Oncol. 2013; 52:963–70. [PubMed: 23514584]
9. Di Nicolantonio, F, Arena, S, Tabernero, J, Grosso, S, Molinari, F, Macarulla, T. , et al. J Clin Invest. Vol. 120. American Society for Clinical Investigation; 2010. Deregulation of the PI3K and KRAS

signaling pathways in human cancer cells determines their response to everolimus; 2858–66. Available from: [Internet]

10. Hung KE, Maricevich MA, Richard LG, Chen WY, Richardson MP, Kunin A, et al. Development of a mouse model for sporadic and metastatic colon tumors and its use in assessing drug treatment. Proc Natl Acad Sci. 2010; 107:1565–1570. [PubMed: 20080688]
11. Park, JH, McMillan, DC, Powell, AG, Richards, CH, Horgan, PG, Edwards, J. , et al. Clin Cancer Res. Vol. 21. United States: 2015. Evaluation of a tumor microenvironment-based prognostic score in primary operable colorectal cancer; 882–8.
12. Truitt ML, Ruggero D. New frontiers in translational control of the cancer genome. Nat Rev Cancer. 2016:288–304. [PubMed: 27112207]
13. Katsumura KR, Yang C, Boyer ME, Li L, Bresnick EH. Molecular basis of crosstalk between oncogenic Ras and the master regulator of hematopoiesis GATA-2. EMBO Rep. 2014; 15:938–947. [PubMed: 25056917]
14. Park M-T, Kim M-J, Suh Y, Kim R-K, Kim H, Lim E-J, et al. Novel signaling axis for ROS generation during K-Ras-induced cellular transformation. Cell Death Differ. 2014; 21:1185–97. [PubMed: 24632950]
15. Morley SJ, McKendrick L. Involvement of Stress-activated Protein Kinase and p38/RK Mitogen-activated Protein Kinase Signaling Pathways in the Enhanced Phosphorylation of Initiation Factor 4E in NIH 3T3 Cells. J Biol Chem. 1997; 272:17887–93. [PubMed: 9211946]
16. Proud CG. Mnks, eIF4E phosphorylation and cancer. Biochim Biophys Acta - Gene Regul Mech. 2015; 1849:766–73.
17. Ueda T, Watanabe-Fukunaga R, Fukuyama H, Nagata S, Fukunaga R. Mnk2 and Mnk1 Are Essential for Constitutive and Inducible Phosphorylation of Eukaryotic Initiation Factor 4E but Not for Cell Growth or Development. Mol Cell Biol. 2004; 24:6539–49. DOI: 10.1128/MCB.24.15.6539-6549.2004 [PubMed: 15254222]
18. Waskiewicz, AJ, Flynn, A, Proud, CG, Cooper, JA. EMBO J. Vol. 16. England: 1997. Mitogen-activated protein kinases activate the serine/threonine kinases Mnk1 and Mnk2; 1909–20.
19. Furic L, Rong L, Larsson O, Koumakpayi IH, Yoshida K, Brueschke A, et al. eIF4E phosphorylation promotes tumorigenesis and is associated with prostate cancer progression. Proc Natl Acad Sci U S A. 2010; 107:14134–9. [PubMed: 20679199]
20. Geter PA, Ernlund AW, Bakogianni S, Alard A, Arju R, Giashuddin S, et al. Hyperactive mTOR and MNK1 phosphorylation of eIF4E confer tamoxifen resistance and estrogen independence through selective mRNA translation reprogramming. Genes Dev. 2017; 31:2235–49. [PubMed: 29269484]
21. Bell JB, Eckerdt FD, Alley K, Magnusson LP, Hussain H, Bi Y, et al. MNK Inhibition Disrupts Mesenchymal Glioma Stem Cells and Prolongs Survival in a Mouse Model of Glioblastoma. Mol Cancer Res. 2016; 14:984–93. DOI: 10.1158/1541-7786.MCR-16-0172 [PubMed: 27364770]
22. Zhan Y, Guo J, Yang W, Goncalves C, Rzymski T, Dreas A, et al. MNK1/2 inhibition limits oncogenicity and metastasis of KIT-mutant melanoma. J Clin Invest. 2017; 127:4179–92. [PubMed: 29035277]
23. Kosciuczuk EM, Saleiro D, Kroczynska B, Beauchamp EM, Eckerdt F, Blyth GT, et al. Merestinib blocks Mnk kinase activity in acute myeloid leukemia progenitors and exhibits antileukemic effects in vitro and in vivo. Blood. 2016; 128:410–4. [PubMed: 27307295]
24. Xu Y, Poggio M, Jin HY, Shi Z, Forester CM, Wang Y, et al. Translation control of the immune checkpoint in cancer and its therapeutic targeting. Nat Med. 2019; 25:301–11. DOI: 10.1038/s41591-018-0321-2 [PubMed: 30643286]
25. Ueda T, Sasaki M, Elia AJ, Chio IIC, Hamada K, Fukunaga R, et al. Combined deficiency for MAP kinase-interacting kinase 1 and 2 (Mnk1 and Mnk2) delays tumor development. Proc Natl Acad Sci. 2010; 107:13984–13990. [PubMed: 20679220]
26. Reich, SH, Sprengeler, PA, Chiang, GG, Appleman, JR, Chen, J, Clarine, J. , et al. J Med Chem. Vol. 61. American Chemical Society; 2018. Structure-based Design of Pyridone–Aminal eFT508 Targeting Dysregulated Translation by Selective Mitogen-activated Protein Kinase Interacting Kinases 1 and 2 (MNK1/2) Inhibition; 3516–40. Available from, [Internet]

27. Scheper GC, van Kollenburg B, Hu J, Luo Y, Goss DJ, Proud CG. Phosphorylation of Eukaryotic Initiation Factor 4E Markedly Reduces Its Affinity for Capped mRNA. J Biol Chem. 2002; 277:3303–9. [PubMed: 11723111]
28. McKendrick, L, Morley, SJ, Pain, VM, Jagus, R, Joshi, B. Eur J Biochem. Vol. 268. John Wiley & Sons, Ltd; 2001. Phosphorylation of eukaryotic initiation factor 4E (eIF4E) at Ser209 is not required for protein synthesis in vitro and in vivo; 5375–85. Available from, [Internet], (10.1111)
29. Sansom, OJ, Meniel, V, Wilkins, JA, Cole, AM, Oien, KA, Marsh, V. , et al. Proc Natl Acad Sci U S A. Vol. 103. National Academy of Sciences; 2006. Sep 07, Loss of Apc allows phenotypic manifestation of the transforming properties of an endogenous K-ras oncogene in vivo; 14122–7. 2006, [Internet], Available from:
30. Haigis KM, Kendall KR, Wang Y, Cheung A, Haigis MC, Glickman JN, et al. Differential effects of oncogenic K-Ras and N-Ras on proliferation, differentiation and tumor progression in the colon. Nat Genet. 2008 Mar 30.40:600–8. [PubMed: 18372904]
31. Poulin EJ, Bera AK, Lu J, Lin Y-J, Strasser SD, Paulo JA, et al. Tissue-Specific Oncogenic Activity of KRAS^{A146T} Cancer Discov. 2019; 9:738–755. [PubMed: 30952657]
32. Raught B, Peiretti F, Gingras AC, Livingstone M, Shahbazian D, Mayeur GL, et al. Phosphorylation of eucaryotic translation initiation factor 4B Ser422 is modulated by S6 kinases. EMBO J. 2004; 23:1761–9. [PubMed: 15071500]
33. Raught B, Gingras AC, Gygi SP, Imataka H, Morino S, Gradi A, et al. Serum-stimulated, rapamycin-sensitive phosphorylation sites in the eukaryotic translation initiation factor 4GI. EMBO J. 2000; 19:434–44. [PubMed: 10654941]
34. Shahbazian, D, Roux, PP, Mieulet, V, Cohen, MS, Raught, B, Taunton, J. , et al. EMBO J. Vol. 25. European Molecular Biology Organization; 2006. The mTOR/PI3K and MAPK pathways converge on eIF4B to control its phosphorylation and activity; 2781–91. Available from, [Internet]
35. Proud, CG. Cold Spring Harb Perspect Biol. Vol. 11. United States: 2019. Phosphorylation and Signal Transduction Pathways in Translational Control.
36. Roper, J, Tammela, T, Cetinbas, NM, Akkad, A, Roghanian, A, Rickelt, S. , et al. Nat Biotechnol. Vol. 35. Nature Publishing Group, a division of Macmillan Publishers Limited; 2017. In vivo genome editing and organoid transplantation models of colorectal cancer and metastasis; 569Available from, All Rights Reserved [Internet]
37. Gay DM, Ridgway RA, Müller M, Hodder MC, Hedley A, Clark W, et al. Loss of BCL9/9l suppresses Wnt driven tumourigenesis in models that recapitulate human cancer. Nat Commun. 2019; 10:723. doi: 10.1038/s41467-019-08586-3 [PubMed: 30760720]
38. Bianchini A, Loiarro M, Bielli P, Busà R, Paronetto MP, Loreni F, et al. Phosphorylation of eIF4E by MNKs supports protein synthesis, cell cycle progression and proliferation in prostate cancer cells. Carcinogenesis. 2008; 29:2279–88. DOI: 10.1093/carcin/bgn221 [PubMed: 18809972]
39. ur Rasool R, Rah B, Amin H, Nayak D, Chakraborty S, Rawoof A, et al. Dual modulation of Ras-Mnk and PI3K-AKT-mTOR pathways: A Novel c-FLIP inhibitory mechanism of 3-AWA mediated translational attenuation through dephosphorylation of eIF4E. Sci Rep. 2016; 6 18800 doi: 10.1038/srep18800 [PubMed: 26728896]
40. Sansom, OJ, Meniel, VS, Muncan, V, Phesse, TJ, Wilkins, JA, Reed, KR. , et al. Nature. Vol. 446. Nature Publishing Group; 2007. Myc deletion rescues Apc deficiency in the small intestine; 676Available from, [Internet]
41. Gildish, I, Manor, D, David, O, Sharma, V, Williams, D, Agarwala, U. , et al. Learn Mem. Vol. 19. Cold Spring Harbor Laboratory Press; 2012. Impaired associative taste learning and abnormal brain activation in kinase-defective eEF2K mice; 116–25. [Internet], Available from
42. Zuberek J, Wyslouch-Ciesyzynska A, Niedzwiecka A, Dadlez M, Stepinski J, Augustyniak W, et al. Phosphorylation of eIF4E attenuates its interaction with mRNA 5′ cap analogs by electrostatic repulsion: Intein-mediated protein ligation strategy to obtain phosphorylated protein. RNA. 2003; 9:52–61. [PubMed: 12554876]
43. Kruspig B, Monteverde T, Neidler S, Hock A, Kerr E, Nixon C, et al. The ERBB network facilitates KRAS-driven lung tumorigenesis. Sci Transl Med. 2018; 10 eaao2565 [PubMed: 29925636]

44. Bruno PM, Liu Y, Park GY, Murai J, Koch CE, Eisen TJ, et al. A subset of platinum-containing chemotherapeutic agents kills cells by inducing ribosome biogenesis stress. Nat Med. 2017 Feb 27.23:461–71. [PubMed: 28263311]
45. Bash-Imam, Z, Thérizols, G, Vincent, A, Lafôrets, F, Polay Espinoza, M, Pion, N. , et al. Oncotarget. Vol. 8. Impact Journals LLC; 2017. Translational reprogramming of colorectal cancer cells induced by 5-fluorouracil through a miRNA-dependent mechanism; 46219–33. [Internet], Available from:
46. Wiegering, A, Uthe, FW, Jamieson, T, Ruoss, Y, Huttenrauch, M, Kuspert, M. , et al. Cancer Discov. Vol. 5. United States: 2015. Targeting Translation Initiation Bypasses Signaling Crosstalk Mechanisms That Maintain High MYC Levels in Colorectal Cancer; 768–81.
47. Fabregat A, Sidiropoulos K, Viteri G, Forner O, Marin-Garcia P, Arnau V, et al. Reactome pathway analysis: a high-performance in-memory approach. BMC Bioinformatics. 2017; 18:142. doi: 10.1186/s12859-017-1559-2 [PubMed: 28249561]
48. Subramanian A, Tamayo P, Mootha VK, Mukherjee S, Ebert BL, Gillette MA, et al. Gene set enrichment analysis: A knowledge-based approach for interpreting genome-wide expression profiles. Proc Natl Acad Sci. 2005; 102:15545–15550. [PubMed: 16199517]
49. Hall Z, Ament Z, Wilson CH, Burkhart DL, Ashmore T, Koulman A, et al. Myc Expression Drives Aberrant Lipid Metabolism in Lung Cancer. Cancer Res. 2016; 76:4608–4618. [PubMed: 27335109]
50. Mohammed, A, Yarla, NS, Madka, V, Rao, CV. Int J Mol Sci. Vol. 19. MDPI; 2018. Clinically Relevant Anti-Inflammatory Agents for Chemoprevention of Colorectal Cancer: New Perspectives. [Internet], Available from:
51. Jackstadt R, van Hooff SR, Leach JD, Cortes-Lavaud X, Lohuis JO, Ridgway RA, et al. Epithelial NOTCH Signaling Rewires the Tumor Microenvironment of Colorectal Cancer to Drive Poor-Prognosis Subtypes and Metastasis. Cancer Cell. 2019; 36:319–336. e7 [PubMed: 31526760]
52. Vlachogiannis G, Hedayat S, Vatsiou A, Jamin Y, Fernández-Mateos J, Khan K, et al. Patient-derived organoids model treatment response of metastatic gastrointestinal cancers. Science (80-). 2018; 359:920–926.
53. Murphy DJ, Junttila MR, Pouyet L, Karnezis A, Shchors K, Bui DA, et al. Distinct Thresholds Govern Myc's Biological Output In Vivo. Cancer Cell. 2008; 14:447–57. [PubMed: 19061836]
54. West, MJ, Stoneley, M, Willis, AE. Oncogene. Vol. 17. England: 1998. Translational induction of the c-myc oncogene via activation of the FRAP/TOR signalling pathway; 769–80.
55. Wall M, Poortinga G, Hannan KM, Pearson RB, Hannan RD, McArthur GA. Translational control of c-MYC by rapamycin promotes terminal myeloid differentiation. Blood. 2008; 112:2305–17. DOI: 10.1182/blood-2007-09-111856 [PubMed: 18621930]
56. Csibi A, Lee G, Yoon S-O, Tong H, Ilter D, Elia I, et al. The mTORC1/S6K1 Pathway Regulates Glutamine Metabolism through the eIF4B-Dependent Control of c-Myc Translation. Curr Biol. 2014; 24:2274–80. [PubMed: 25220053]
57. Shi, Y, Frost, P, Hoang, B, Yang, Y, Fukunaga, R, Gera, J. , et al. Oncogene. Vol. 32. England: 2013. MNK kinases facilitate c-myc IRES activity in rapamycin-treated multiple myeloma cells; 190–7.
58. Schmidt S, Gay D, Uthe FW, Denk S, Paauwe M, Matthes N, et al. A MYC–GCN2-eIF2α negative feedback loop limits protein synthesis to prevent MYC-dependent apoptosis in colorectal cancer. Nat Cell Biol. 2019; 21:1413–24. DOI: 10.1038/s41556-019-0408-0 [PubMed: 31685988]
59. Lineham, E, Tizzard, GJ, Coles, SJ, Spencer, J, Morley, SJ. Oncotarget. Vol. 9. United States: 2018. Synergistic effects of inhibiting the MNK-eIF4E and PI3K/AKT/ mTOR pathways on cell migration in MDA-MB-231 cells; 14148–59.
60. Marzec, M, Liu, X, Wysocka, M, Rook, AH, Odum, N, Wasik, MA. PLoS One. Vol. 6. Public Library of Science; 2011. Simultaneous Inhibition of mTOR-Containing Complex 1 (mTORC1) and MNK Induces Apoptosis of Cutaneous T-Cell Lymphoma (CTCL) Cells. Available from, [Internet]
61. Altman JK, Szilard A, Konicek BW, Iversen PW, Kroczynska B, Glaser H, et al. Inhibition of Mnk kinase activity by cercosporamide and suppressive effects on acute myeloid leukemia precursors. Blood. 2013; 121:3685–3681.

62. Wen, Q, Wang, W, Luo, J, Chu, S, Chen, L, Xu, L. , et al. Oncotarget. Vol. 7. United States: 2016. CGP57380 enhances efficacy of RAD001 in non-small cell lung cancer through abrogating mTOR inhibition-induced phosphorylation of eIF4E and activating mitochondrial apoptotic pathway; 27787–801.

63. Lock, R, Ingraham, R, Maertens, O, Miller, AL, Weledji, N, Legius, E. , et al. J Clin Invest. Vol. 126. United States: 2016. Cotargeting MNK and MEK kinases induces the regression of NF1-mutant cancers; 2181–90.

64. Fortin, CF, Mayer, TZ, Cloutier, A, McDonald, PP. J Leukoc Biol. Vol. 94. United States: 2013. Translational control of human neutrophil responses by MNK1; 693–703.

65. Buxade, M, Parra, JL, Rousseau, S, Shpiro, N, Marquez, R, Morrice, N. , et al. Immunity. Vol. 23. United States: 2005. The Mnks are novel components in the control of TNF alpha biosynthesis and phosphorylate and regulate hnRNP A1; 177–89.

66. Robichaud N, Hsu BE, Istomine R, Alvarez F, Blagih J, Ma EH, et al. Translational control in the tumor microenvironment promotes lung metastasis: Phosphorylation of eIF4E in neutrophils. Proc Natl Acad Sci. 2018; 115:E2202–9. DOI: 10.1073/pnas.1717439115 [PubMed: 29463754]

67. Fan, S, Ramalingam, SS, Kauh, J, Xu, Z, Khuri, FR, Sun, S-Y. Cancer Biol Ther. Vol. 8. Taylor & Francis; 2009. Phosphorylated eukaryotic translation initiation factor 4 (eIF4E) is elevated in human cancer tissues; 1463–9. Available from, [Internet]

68. Network TCGA. Comprehensive genomic characterization of head and neck squamous cell carcinomas. Nature. 2015; 517:576. doi: 10.1038/nature14129 [PubMed: 25631445]

69. Network TCGAR. Comprehensive molecular profiling of lung adenocarcinoma. Nature. 2014; 511:543. doi: 10.1038/nature13385 [PubMed: 25079552]

70. El Marjou F, Janssen KP, Chang BHJ, Li M, Hindie V, Chan L, et al. Tissue-specific and inducible Cre-mediated recombination in the gut epithelium. Genesis. 2004; 39:186–93. [PubMed: 15282745]

71. Fisher S, Barry A, Abreu J, Minie B, Nolan J, Delorey TM, et al. A scalable, fully automated process for construction of sequence-ready human exome targeted capture libraries. Genome Biol. 2011; 12 R1 doi: 10.1186/gb-2011-12-1-r1 [PubMed: 21205303]

Europe PMC Funders Author Manuscripts

Europe PMC Funders Author Manuscripts

Statement of significance

KRAS mutation and elevated c-MYC are widespread in many tumors but remain predominantly un-targetable. We find that mutant *KRAS* modulates translation, culminating in increased expression of c-MYC. We describe an effective strategy targeting mTORC1 and MNK in *KRAS*-mutant mouse and human models, pathways which are also commonly co-upregulated in CRC.

Europe PMC Funders Author Manuscripts

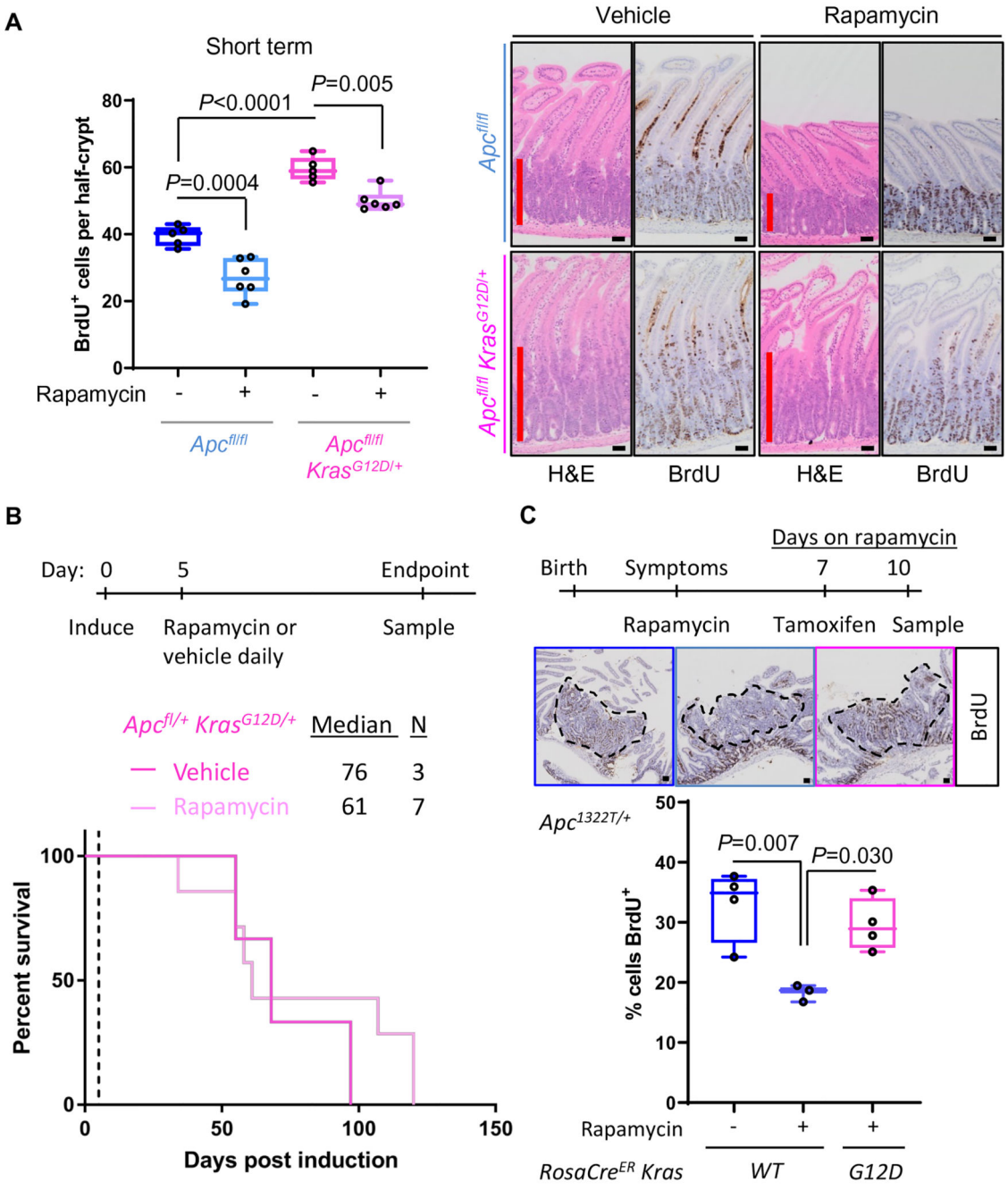

Figure 1. Oncogenic KRAS results in aggressive rapamycin-resistant *Apc*-deficient tumor models

(A) Left, BrdU incorporation in the small intestine of vehicle- or rapamycin-treated $Apc^{fl/fl}$ and $Apc^{fl/fl}$ $Kras^{G12D/+}$ short-term model mice at 4- and 3-days post induction, respectively. Mice were injected with BrdU 2hours prior to sampling. ≥25 half crypts were counted per mouse with each point representing a biological replicate. *P* values are from one-way ANOVA Tukey's multiple comparisons tests. Right, micrographs show representative H&E and BrdU staining. Red line marks the extent of the proliferative zone. (B) Top, schematic of treatment timeline. Bottom, survival of $Apc^{fl/+}$ $Kras^{G12D/+}$ tumor model mice treated with

rapamycin or vehicle daily from 5days post-induction. (C) Top, schematic of treatment timeline. BrdU incorporation scored in small intestinal tumors from $Apc^{1322T/+}$ mice treated with rapamycin for 10days, with and without $Rosa^{CreER}$ driven $KRAS^{G12D}$ activation 7days after starting rapamycin. The average % BrdU positivity was scored in ≥2 adenomas per mouse with each point representing a biological replicate. *P* values are from one-way ANOVA Tukey's multiple comparisons tests. Representative images of tumors (dashed lines) stained for BrdU antibody are shown. Proliferation in untreated mice is shown for comparison (left bar). All data are represented as mean ± S.E.M. Scale bars, 50μm. See also Figure S1.

Europe PMC Funders Author Manuscripts

Europe PMC Funders Author Manuscripts

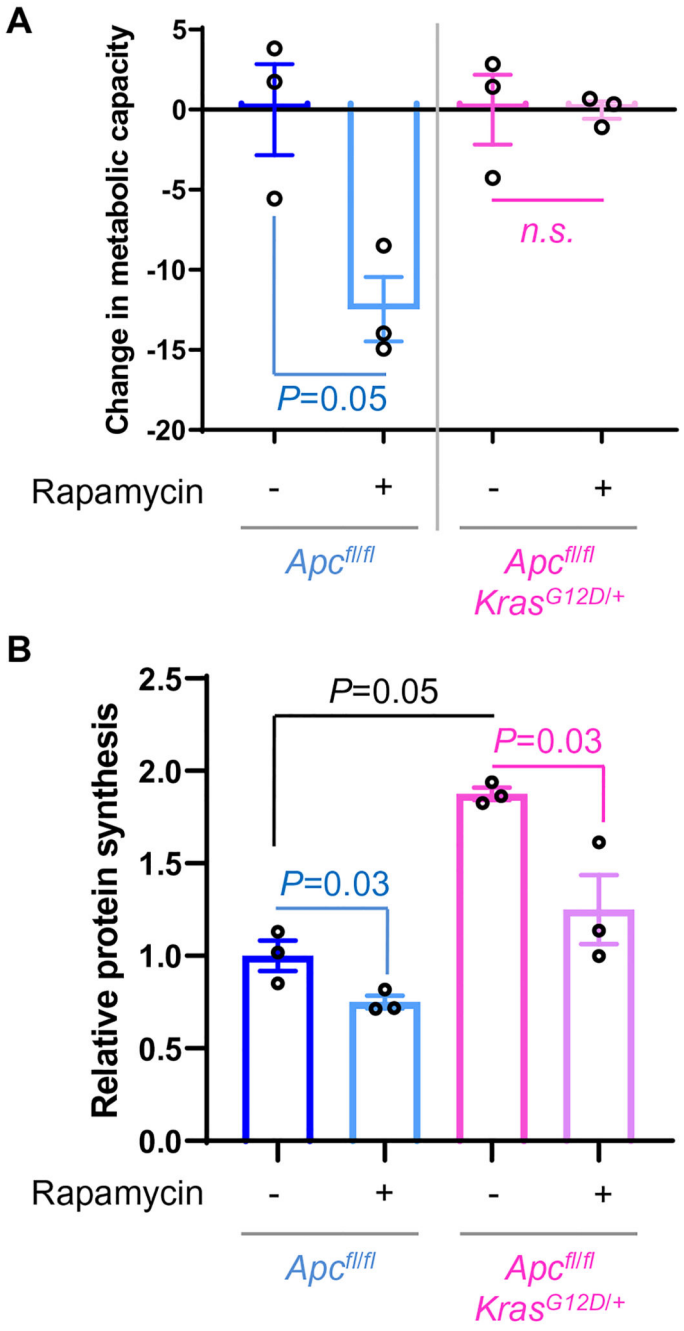

Figure 2. Translation and proliferation are uncoupled following *Kras* mutation

(A) Growth of $Apc^{fl/fl}$ or $Apc^{fl/fl}$ $Kras^{G12D/+}$ organoids, following 30hour treatment with 1μM rapamycin, relative to vehicle-treated organoids. Technical triplicates were performed and averaged to show the biological replicates as plotted. *P* values are from paired student t tests. The relative growth for untreated $Apc^{fl/fl}$ and $Apc^{fl/fl}$ $Kras^{G12D/+}$organoids is set as 0. (B) Protein synthesis in small intestinal organoids of the indicated genotypes following 6hours of treatment with 250nM rapamycin or vehicle. Values are from 3 independent

biological replicates ±SEM, represented relative to $Apc^{fl/fl}$ vehicle treated organoids. *P* values are from paired student t tests or a Mann Whitney test. See also Figure S2.

Europe PMC Funders Author Manuscripts

Europe PMC Funders Author Manuscripts

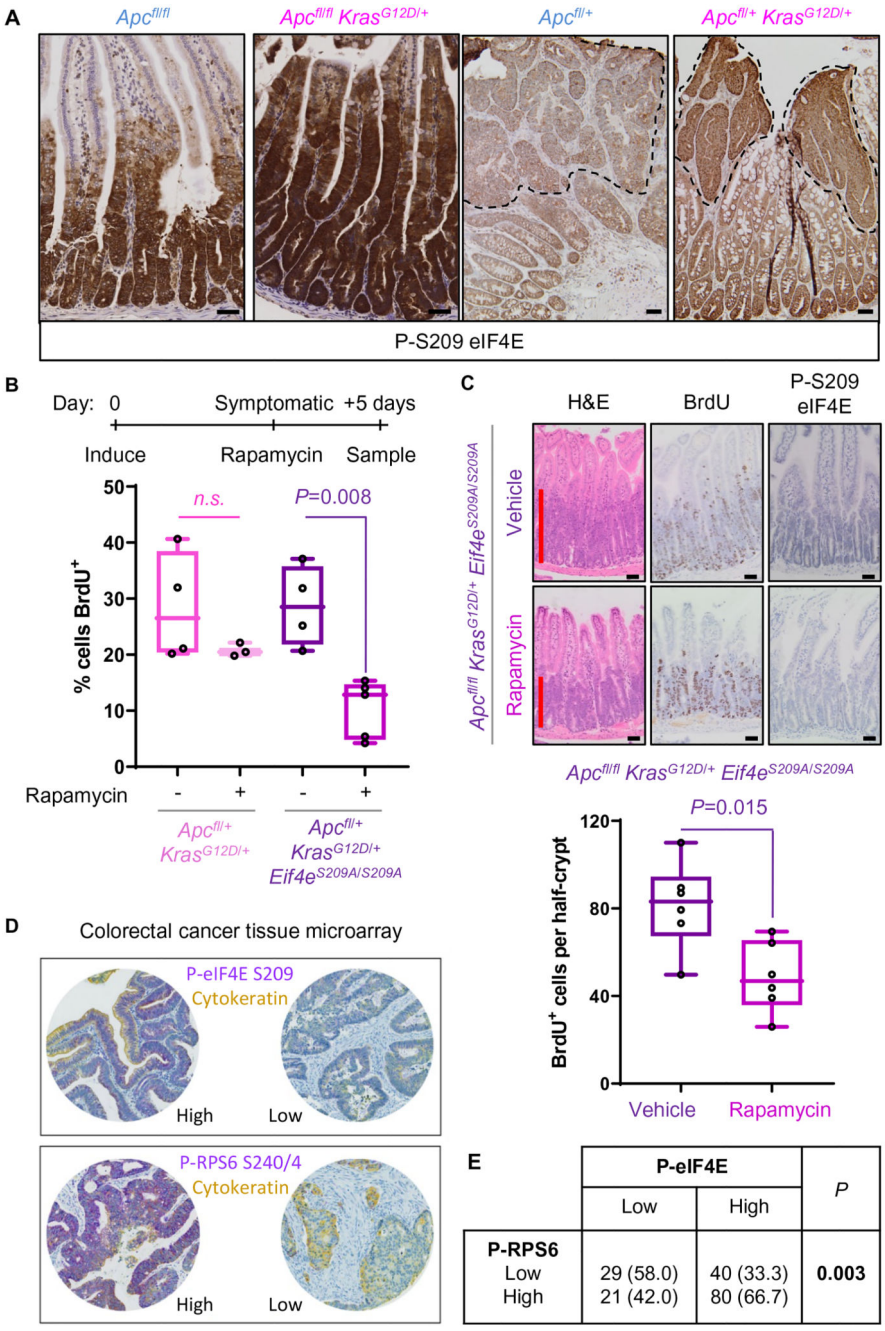

E

	P-eIF4E		P
	Low	High	
P-RPS6			
Low	29 (58.0)	40 (33.3)	**0.003**
High	21 (42.0)	80 (66.7)	

Figure 3. P-eIF4E is increased by *Kras* mutation and synergizes with mTORC1 to promote proliferation

(A) Immunohistochemistry (IHC) staining for P-eIF4E in short-term model (left 2 panels) and tumor model colonic adenomas (right 2 panels) from $Apc^{fl/fl\ or\ +}$ and $Apc^{fl/fl\ or\ +}$ $Kras^{G12D/+}$ mice. Dashed line denotes adenoma boundary. Images are representative of ≥3 biological replicates. (B) Top, schematic of treatment timeline. $Apc^{fl/+}$ $Kras^{G12D/+}$ and $Apc^{fl/+}$ $Kras^{G12D/+}$ $Eif4e^{S209A/S209A}$ tumor model mice were allowed to develop symptoms of intestinal tumors, treated with rapamycin for 5days, and then sampled 2hours after BrdU administration. Bottom, BrdU incorporation into colonic epithelial adenoma cells quantified

from a minimum of 4 tumors per mouse, with each point representing a biological replicate *P* values are from one-way ANOVA Tukey's multiple comparisons tests (C) Bottom, quantification of BrdU incorporation in $Apc^{fl/fl}$ $Kras^{G12D/+}$ $Eif4e^{S209A/S209A}$ short-term model mice treated with rapamycin or vehicle. Top, representative H&E, BrdU and P-eIF4E staining for each treatment, with red bar showing extent of proliferation. ≥25 half crypts were quantified per mouse, with the average for each mouse plotted in the figure. *P* value is from a Mann Whitney test. (D) Representative images of staining for P-eIF4E and P-RPS6 each duplexed with cytokeratin from a TMA of colorectal cancer patients. Examples of high and low staining are shown for each. (E) Correlation between P-eIF4E and P-RPS6 from the TMA shown in (D). Significance was tested using X^2-test. All data are represented as mean ± S.E.M. Scale bars, 50μm. See also Figure S3.

Europe PMC Funders Author Manuscripts

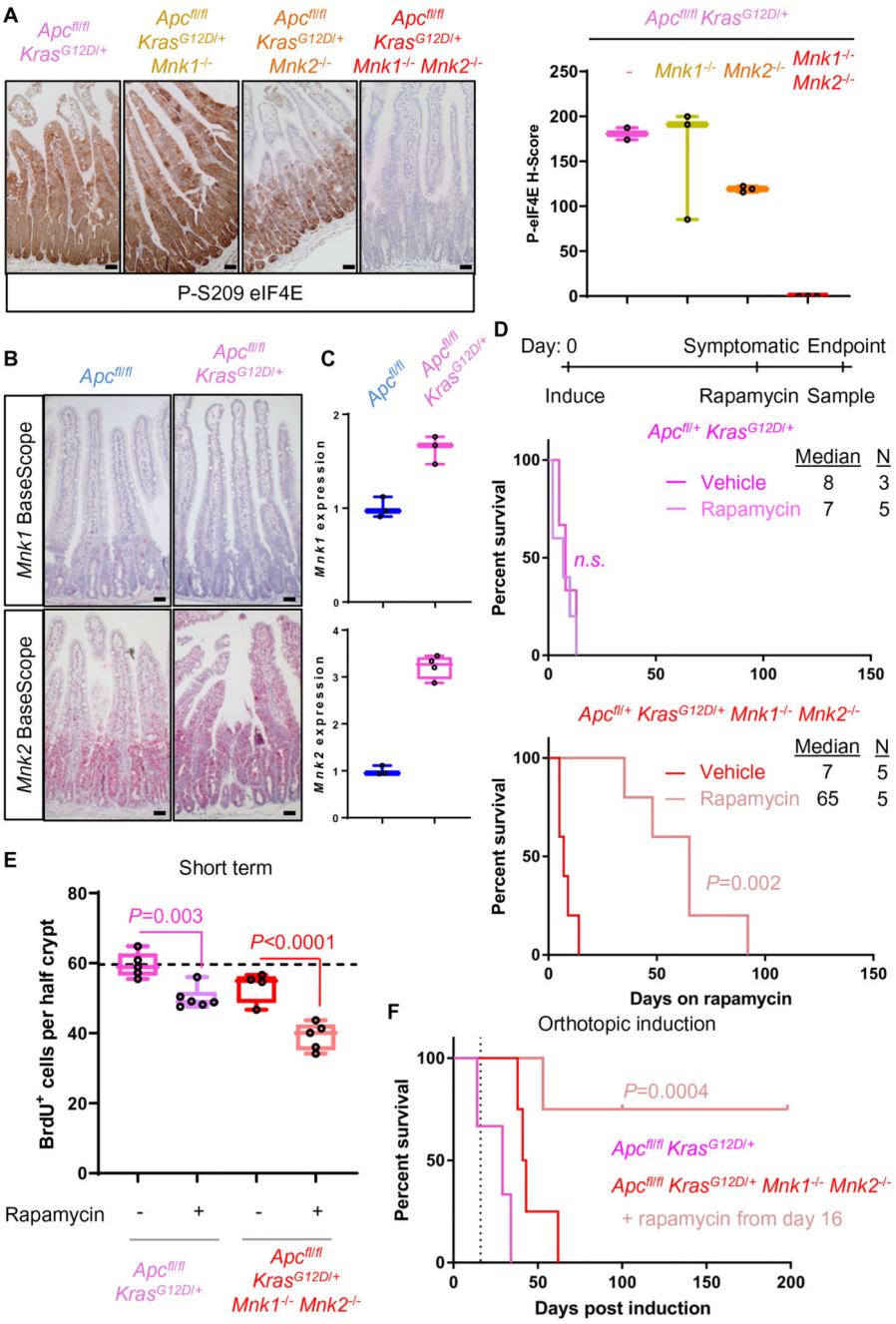

Figure 4. *Mnk* deletion suppresses mutant *KRAS*-driven tumor proliferation in combination with rapamycin treatment

(A) IHC for P-eIF4E in the small intestine of $Apc^{fl/fl}$ $Kras^{G12D/+}$ short-term model mice with deletion of *Mnk1*, *Mnk2* or both *Mnk1* and *Mnk2*. Right, quantification of this P-eIF4E staining. (B) BaseScope analysis of *Mnk1* and *Mnk2* expression in $Apc^{fl/fl}$ and $Apc^{fl/fl}$ $Kras^{G12D/+}$ small intestines. (C) qPCR for *Mnk1* and *Mnk2* in $Apc^{fl/fl}$ and $Apc^{fl/fl}$ $Kras^{G12D/+}$ small intestines. Levels are expressed relative to *Actb* mRNA expression. (D) Top, schematic of treatment timeline. $Apc^{fl/+}$ $Kras^{G12D/+}$ and $Apc^{fl/+}$ $Kras^{G12D/+}$ $Mnk1^{-/-}$ $Mnk2^{-/-}$ tumor model mice were aged until symptoms of intestinal tumors, and then treated

with rapamycin or vehicle until endpoint. Survival is plotted as the number of days on rapamycin or vehicle treatment. *P* value is from a Log-rank Mantel-Cox test. (E) BrdU incorporation scored from small intestines of $Apc^{fl/fl}$ $Kras^{G12D/+}$ and $Apc^{fl/fl}$ $Kras^{G12D/+}$ $Mnk1^{-/-}$ $Mnk2^{-/-}$ short-term model mice, treated with and without rapamycin. $Apc^{fl/fl}$ $Kras^{G12D/+}$ data are reproduced from Figure 1A, for ease of comparison. ≥25 half crypts were quantified per mouse, with the average for each mouse plotted in the figure shown. *P* values are from one-way ANOVA Tukey's multiple comparisons tests. Horizontal line represents the average for $Apc^{fl/fl}$ $Kras^{G12D/+}$ mice. (F) Survival plot following orthotopic induction in the distal colon of $Apc^{fl/fl}$ $Kras^{G12D/+}$ (n=3) or $Apc^{fl/fl}$ $Kras^{G12D/+}$ $Mnk1^{-/-}$ $Mnk2^{-/-}$ mice (n=4). A cohort of $Apc^{fl/fl}$ $Kras^{G12D/+}$ $Mnk1^{-/-}$ $Mnk2^{-/-}$ mice was also treated with rapamycin from day 16 (n=4), indicated by vertical dashed line. Colonic polyps were imaged by colonoscopy on the days shown. *P* value is from a Log-rank Mantel-Cox test. An $Apc^{fl/fl}$ $Kras^{G12D/+}$ $Mnk1^{-/-}$ $Mnk2^{-/-}$ mouse on rapamycin was censored at 100days post induction not related to procedure and two were censored at the end of study at 202days post induction. All data are represented as mean ± S.E.M. Scale bars, 50μm. See also Figure S4.

Europe PMC Funders Author Manuscripts

Europe PMC Funders Author Manuscripts

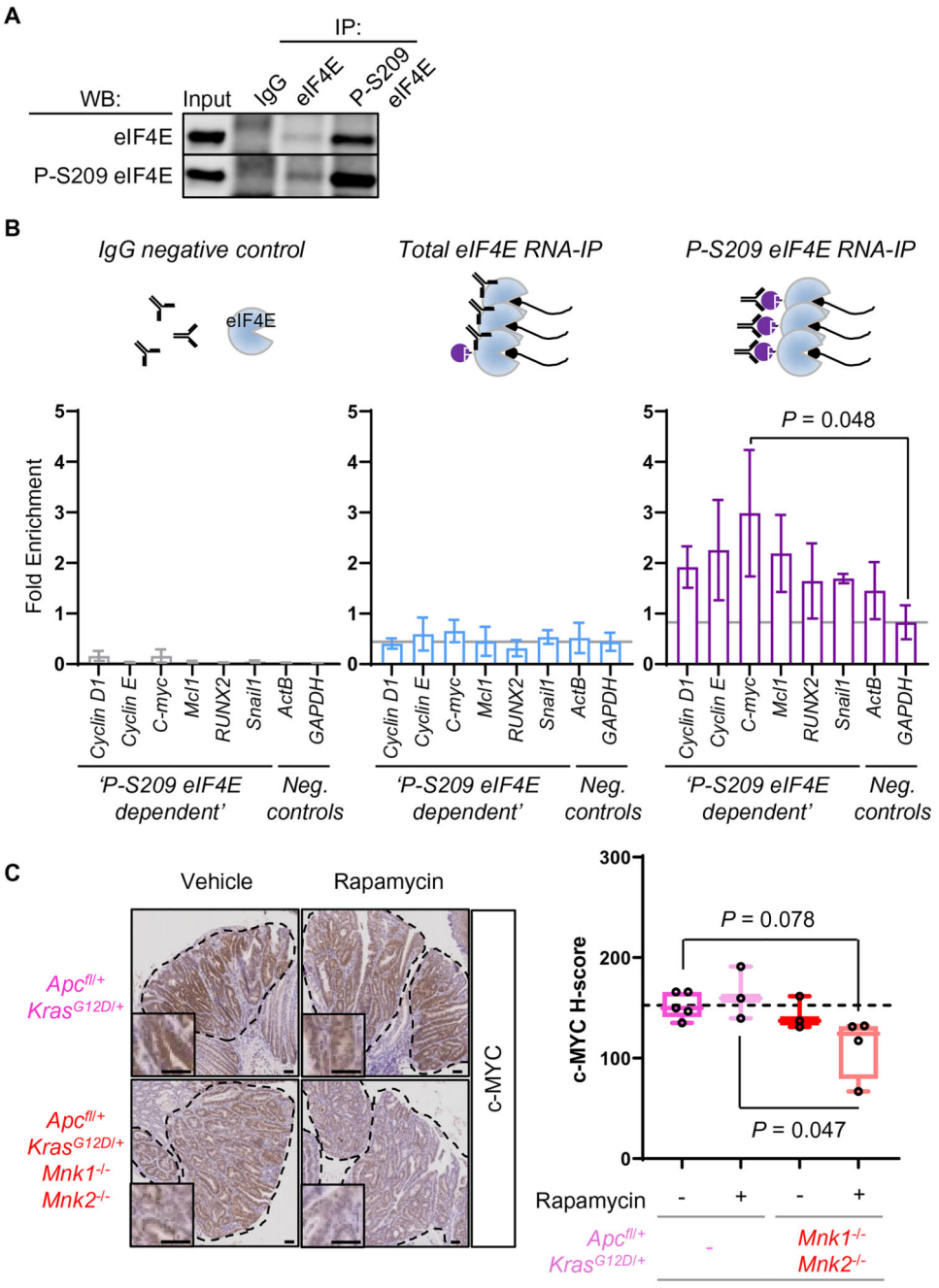

Figure 5. Translation of *C-myc* requires P-eIF4E and active mTORC1 signaling

(A) Validation of immunoprecipitation (IP) of total eIF4E or P-eIF4E by western blotting (WB) for each respective target. (B) Top, schematic showing that total eIF4E antibody precipitates both phosphorylated and non-phosphorylated eIF4E, whereas P-S209 eIF4E antibody specifically precipitates the phosphorylated form. Bottom, qPCR for mRNA targets using RNA eluted from the eIF4E, P-S209 eIF4E IPs or IgG control precipitation which eluted no eIF4E. Data are plotted as the linearized Ct values for the RNA IP subtracted from the Ct value for the Input. The grey line in each graph is value for the *Gapdh* transcript. All

data are the average of 4 biological replicates. Significance was tested by paired student t test (C) IHC for c-MYC in adenomas from $Apc^{fl/+}$ $Kras^{G12D/+}$ or $Apc^{fl/+}$ $Kras^{G12D/+}$ $Mnk1^{-/-}$ $Mnk2^{-/-}$ mice treated with or without rapamycin for 5days prior to sampling. Staining intensity was quantified using nuclear c-MYC H-scores shown in the adjacent graph. The average H-score from at least 7 adenomas per mouse, with each point shown a biological replicate. *P* values are from one-way ANOVA Tukey's multiple comparisons tests. All data are represented as mean ± S.E.M. Scale bars, 50μm. See also Figure S5.

Europe PMC Funders Author Manuscripts

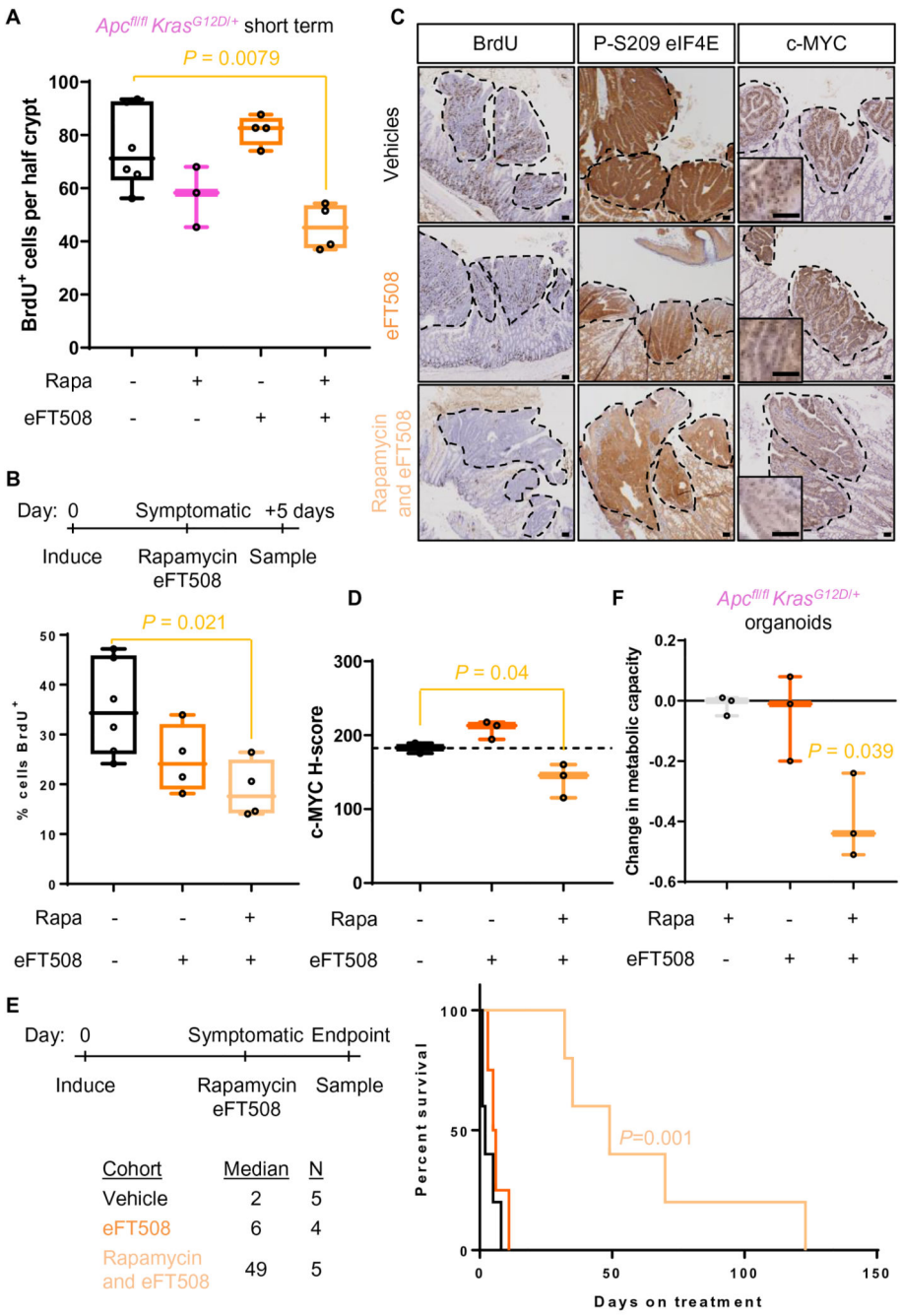

Figure 6. Targeting the MNKs with eFT508 combines with rapamycin to suppress the APC KRAS phenotype

(A) BrdU incorporation in *Apc*$^{fl/fl}$ *Kras*$^{G12D/+}$ short-term model mice treated with eFT508 or eFT508 in combination with rapamycin. ≥25 half crypts were quantified per mouse, with the average for each mouse plotted in the figure shown. *P* value is from one-way ANOVA Tukey's multiple comparisons tests. (B) *Apc*$^{fl/+}$ *Kras*$^{G12D/+}$ tumor model mice were treated with eFT508 alone, or in combination with rapamycin for 5days, after presenting with symptoms of intestinal adenomas. BrdU was administered 2hours prior to sampling then the percentage of BrdU-positive adenoma cells was quantified. ≥5 adenomas were analyzed per

mouse then the average of these plotted in the graph. Each point represents a biological replicate. *P* value is from one-way ANOVA Tukey's multiple comparisons tests. (C) Micrographs showing representative staining for BrdU incorporation and P-eIF4E and c-MYC levels from (B). (D) Quantification of c-MYC staining in (C) by H-score. *P* value is from one-way ANOVA Tukey's multiple comparisons tests. (E) Left, schematic of treatment timeline. Right, $Apc^{fl/+}$ $Kras^{G12D/+}$ tumor model mice treated as in (B) and allowed to age on treatment until clinical endpoint. P value is from a Log-rank Mantel-Cox test. (F) $Apc^{fl/fl}$ $Kras^{G12D/+}$ organoids were treated with eFT508 (30nM) or eFT508 in combination with rapamycin (250nM) for 24hours, and the change in growth compared with vehicle-treated cells. Each data point represents an independent biological replicate, which is the average of 3 technical triplicates. *P* value is from a paired student t test. All data are represented as mean ± S.E.M. Scale bars, 50μm. See also Figure S6.

Europe PMC Funders Author Manuscripts

Europe PMC Funders Author Manuscripts

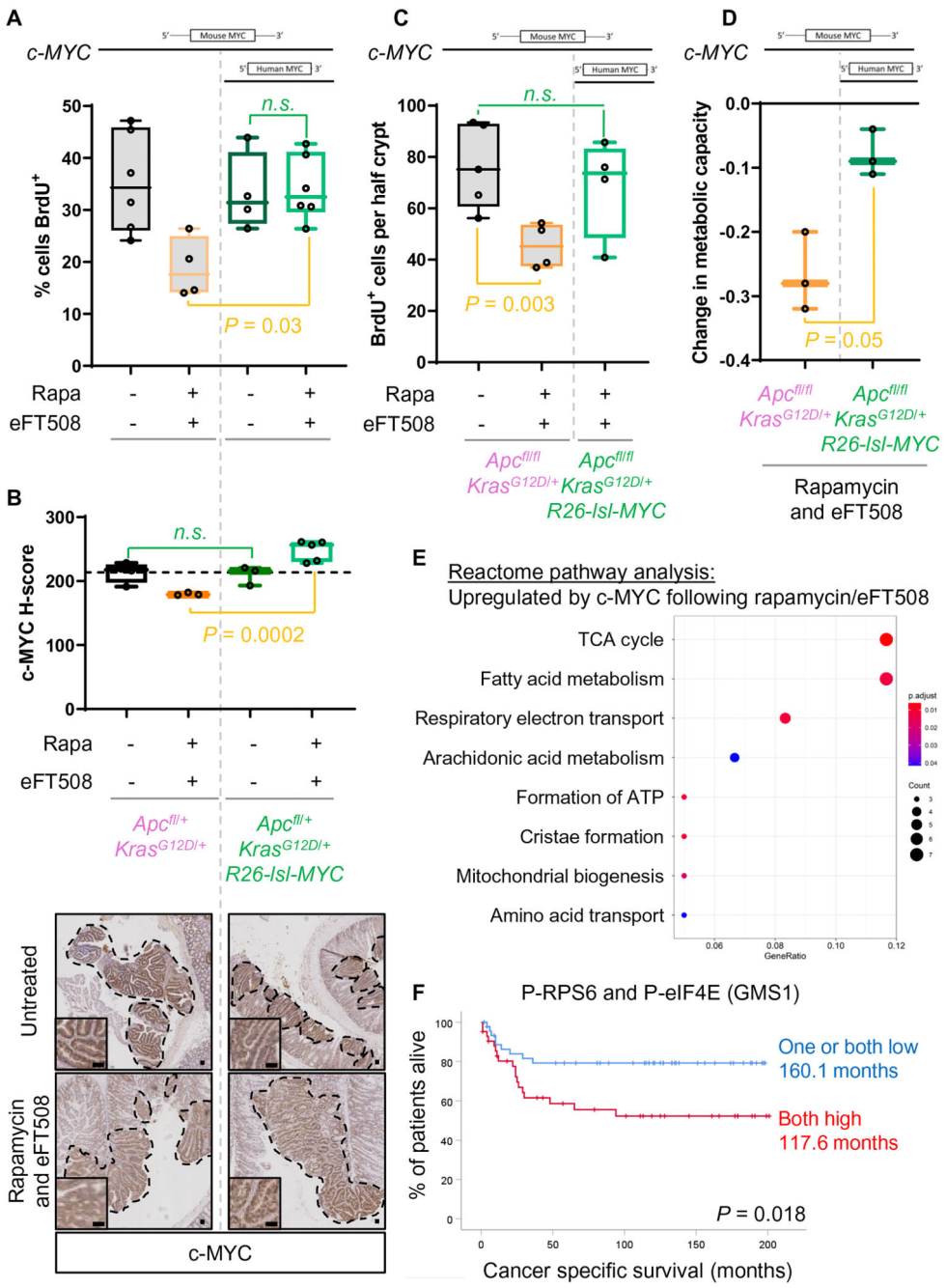

Figure 7. Expression of a human *C-MYC* transgene completely reverses the beneficial effect of eFT508/rapamycin treatment *in vivo*.

(A) Top, indicator of c-MYC variants expressed. *Apc*$^{fl/+}$ *Kras*$^{G12D/+}$ *R26-lsl-MYC* tumor model mice were treated with eFT508 in combination with rapamycin for 5days after presenting with symptoms of intestinal adenomas. BrdU was administered 2hours prior to sampling and the percentage of BrdU-positive adenoma cells quantified. Data for *Apc*$^{fl/+}$ *Kras*$^{G12D/+}$ control mice are reproduced from Figure 6B for ease of comparison. % BrdU positivity was averaged in at least 5 adenomas per mouse, with each point representing an individual mouse. *P* values are from one-way ANOVA Tukey's multiple comparisons tests.

Europe PMC Funders Author Manuscripts

(B) c-MYC staining (bottom) and H-score quantification (top) in adenomas from *Apc*$^{fl/+}$ *Kras*$^{G12D/+}$ and *Apc*$^{fl/+}$ *Kras*$^{G12D/+}$ *R26-lsl-MYC* tumor model mice after 5days of treatment with eFT508/rapamycin. C-MYC H-Score was determined for ≥7 adenomas per mouse then the average plotted on the graph shown. *P* values are from one-way ANOVA Tukey's multiple comparisons tests. (C) Top, indicator of c-MYC variants expressed. BrdU incorporation in *Apc*$^{fl/fl}$ *Kras*$^{G12D/+}$ *R26-lsl-MYC* short-term model mice treated with eFT508 in combination with rapamycin. BrdU incorporation values for *Apc*$^{fl/fl}$ *Kras*$^{G12D/+}$ mice treated with eFT508/rapamycin are reproduced from Figure 6A. ≥25 half crypts were scored per mouse then the average plotted as an individual point on the graph. *P* values are from one-way ANOVA Tukey's multiple comparisons tests. (D) Top, indicator of c-MYC variants expressed. Growth of *Apc*$^{fl/fl}$ *Kras*$^{G12D/+}$ or *Apc*$^{fl/fl}$ *Kras*$^{G12D/+}$ *R26-lsl-MYC* organoids treated with eFT508 (30nM) and rapamycin (250nM) for 24hours compared to growth of vehicle-treated counterparts. Technical triplicates were averaged for 3 independent organoid lines, with these average values represented by each point on the graph. *P* value is from paired student t test. (E) REACTOME pathway plot showing significantly positively enriched pathways in RNA sequencing between rapamycin/eFT508 treated *Apc*$^{fl/fl}$ *Kras*$^{G12D/+}$ *R26-lsl-MYC* compared to *Apc*$^{fl/fl}$ *Kras*$^{G12D/+}$ intestines. The gene ratio indicates the fraction of genes in a pathway that are regulated, with the absolute number shown by circle size. The circle color indicates the significance of enrichment. (F) Kaplan-Meier survival curve of cancer-specific survival for GMS1 patients staining low for one or both of P-RPS6 S240/4 and P-eIF4E S209 (n=46) compared to those staining high for both markers (n=42). Median survival is annotated on each line. Significance was determined by Log-Rank test. All data are represented as mean ± S.E.M. Scale bars, 50μm. See also Figure S7.